Nuclear Energy Research Initiative (NERI)
Final Scientific/Technical Report

"Developing Improved Structural Materials using Proton Irradiation as a Rapid Analysis Tool"

Project IWO # M2SF 02-110
Project No. 99-0155

Submitted by:
Lead Organization: Argonne National Laboratory
Todd R. Allen

Collaborating Organizations:
University of Michigan

Submitted on:

30 April 2003

Available electronically at http://www.doe.gov/bridge

Available for a processing fee to U.S. Department of Energy and its contractors, in paper, from:

U.S. Department of Energy
Office of Scientific and Technical Information
P.O. Box 62
Oak Ridge, TN 37831-0062
phone: (865) 576-8401
fax: (865) 576-5728
email: reports@adonis.osti.gov

Table of Contents

Figures

Tables

Executive Summary

Research Objective

The overall goal of the project is to develop austenitic stainless steel structural materials with enhanced radiation resistance. For this project, the term radiation resistance is being used to describe resistance to dimensional changes caused by void swelling and resistance to material failures caused by irradiation assisted stress corrosion cracking (IASCC). IASCC has been linked to both hardening and changes in grain boundary composition during irradiation. To achieve such enhanced radiation resistance, three experimental paths have been chosen: bulk composition engineering, grain boundary composition engineering, and grain boundary structural engineering. The program involves the use of high-energy proton irradiation as a rapid screening tool to systematically test combinations of alloy composition and thermomechanical treatment conditions to isolate the controlling mechanisms and develop an understanding of how these factors can be engineered to improve material properties.

The alloys chosen for the study have been modeled after commercially available grades of stainless steel commonly used in reactor applications. The model alloys include the following nominal compositions: Fe-18Cr-8Ni-1.75Mn (base 304), Fe-18Cr-40Ni-1.25Mn (Base 330), Fe-18Cr-9.5Ni-1.25Mn + Zr additions (Base 304 + Zr), Fe-16Cr-13Ni-1.25Mn (Base 316), Fe-16Cr-13Ni-1.25Mn +Mo (Base 316 + Mo), Fe-16Cr-13Ni-1.25Mn +Mo + P (Base 316 + Mo + P). Each of the alloying additions was chosen for a specific purpose. Fe-18Cr-40Ni-1.25Mn was chosen because higher bulk nickel concentration is known to reduce swelling, but its affect on IASCC is unknown. Fe-18Cr-8Ni-1.25Mn+Zr alloys were chosen because Zr is an oversized element that might trap point defects and prevent swelling, grain boundary segregation, and other radiation damage. Fe-16Cr-13Ni-1.25Mn, Fe-16Cr-13Ni-1.25Mn+Mo, and Fe-16Cr-13Ni-1.25Mn+Mo+P were chosen to determine why 316 stainless steel is more resistant to swelling and IASCC than 304 stainless steel. The alloys are naturally classified in three groups: the “316 series” (Fe-16Cr-13Ni-1.25Mn, Fe-16Cr-13Ni-1.25Mn+Mo, and Fe-16Cr-13Ni-1.25Mn+Mo+P), the “Zr series” (Fe-18Cr-8Ni-1.75Mn and Fe-18Cr-8Ni-1.75Mn+Zr), and the “Ni-series” (Fe-18Cr-8Ni-1.75Mn, Fe-16Cr-13Ni-1.25Mn, and Fe-18Cr-40Ni-1.25Mn).

Research Progress

In the first year of the project, the bulk composition engineering path was emphasized. Fe-18Cr-8Ni-1.25Mn, Fe-18Cr-40Ni-1.25Mn, Fe-18Cr-8Ni-1.25Mn+Zr, and Fe-16Cr-13Ni-1.25Mn were studied to determine the effect of bulk composition on swelling and radiation-induced segregation (RIS) at grain boundaries. Samples were irradiated using 3.2 MeV protons at 400°C to 1 displacement per atom (dpa). Swelling was characterized by measuring the void size distribution using a transmission electron microscope (TEM). Radiation-induced grain boundary segregation was measured using a field emission gun scanning transmission electron microscope (FEG-STEM). Microhardness measurements were performed on irradiated and non-irradiated alloys to estimate the effect of irradiation on strength.

Results revealed that alloys with greater bulk nickel concentration have greater radiation induced segregation (RIS). They also have increased hardening and Cr depletion, theoretically making the alloy more susceptible to IASCC. Molybdenum additions did not have a significant impact on the swelling and RIS behavior of the 316 series model alloys, but the addition of phosphorus led to a substantial refinement of the dislocation microstructure, suppression of void formation, and a reduction in the extent of Cr depletion at grain boundaries.

During the second year of the project, the effect of pre-irradiation heat treatments on thermal non-equilibrium grain boundary segregation and subsequent radiation-induced grain boundary segregation in the 316 series of model austenitic stainless steels was studied as part of the grain boundary composition engineering path. The alloys were heat treated at temperatures ranging from 1100 to 1300°C and quenched using four different cooling paths (furnace cool, air cool, water quench and ice brine quench) to evaluate the effect of annealing temperature and cooling rate on pre-irradiation grain boundary chemistry. Subsequent RIS behavior following irradiation with high-energy protons was characterized to understand the influence of alloying additions and pre-irradiation grain boundary chemistry in irradiation-induced elemental enrichment and depletion profiles. The study reveals that faster cooling rates provided by water and salt-brine quenching resulted in moderate Cr enrichment. However, slower cooling rates provided by both air and furnace cooling led to more substantial grain boundary enrichment of Cr, Mo and

depletion of Ni, and Fe. Figure 1 illustrates the change in Cr and Mo enrichment as a function of cooling rate. Lower annealing temperatures also tended to enhance the degree of boundary enrichment. Subsequent proton irradiation of the Fe-16Cr-13Ni + Mo alloy following heat treatments to enrich the grain boundary resulted in the formation of a W shaped Cr segregation profile and a reduction in the extent of Cr depletion.

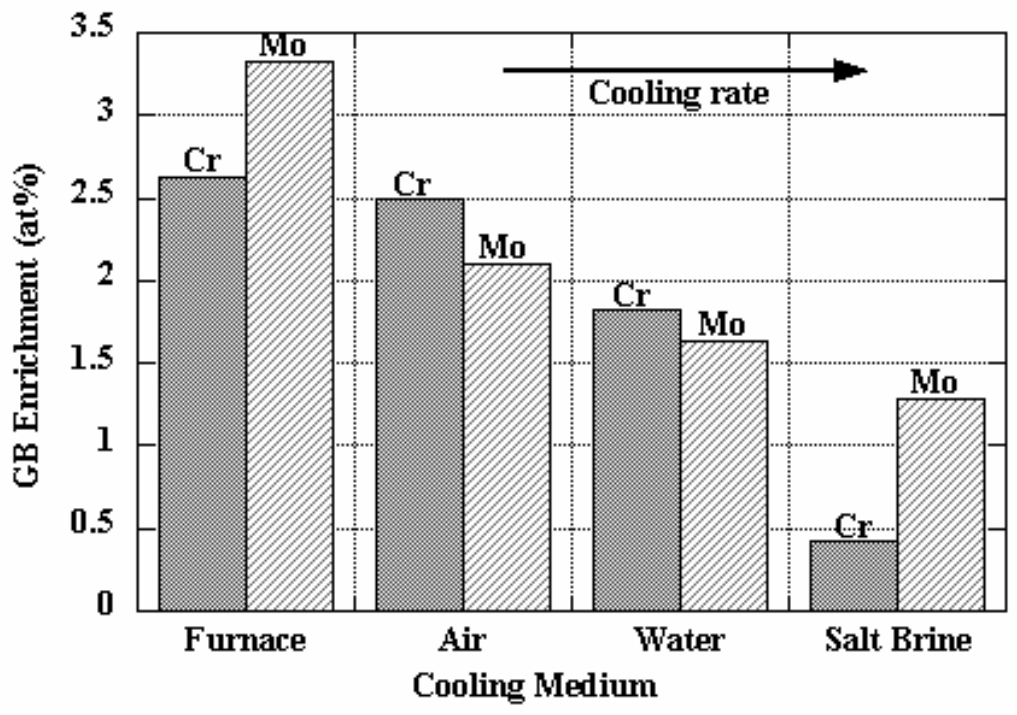

Figure 1 Effect of cooling rate on extent of grain boundary elemental enrichment in Fe-16Cr-13Ni + Mo + P annealed at 1200°C for 1 hour.

Formation of vacancy concentrations during higher temperature annealing and their subsequent migration to sinks during cooling is believed to be the primary process leading to the enrichment of solute species at grain boundaries. Grain boundaries act as sinks for vacancies during cooldown, and the vacancies can drag the solute and thus enrich the boundaries. Models that have been used to describe and explain this include terms for the diffusion of vacancies and vacancy solute complexes to the grain boundary and an associated back diffusion of free-solutes that limits the overall amount of segregation. However current models do not adequately predict the subsequent segregation behavior during irradiation and the result of this study may provide additional insight into these processes.

In the third year, the radiation response in the 304 plus Zr alloys and the 316 plus grain boundary composition engineering samples was analyzed. Following proton radiation, hardness was measured and microstructures were characterized. The addition of Zr decreased the hardening, reduced the swelling (figure 2), reduced the density of radiation-induced void and dislocation loops, and increased the radiation-induced grain boundary segregation. The Zr additions appear to be greater improvement in radiation resistance than the increases in nickel concentration pursued in year 1. Both treatments reduced the swelling, but the Zr-doped alloys did so with out an associated increase in hardening. The 316 plus grain boundary composition engineering delayed the Cr depletion that occurs under irradiation as compared to the non-treated samples. This treatment alone does not provide radiation resistance but may be combined with other treatments to create a more optimal situation.

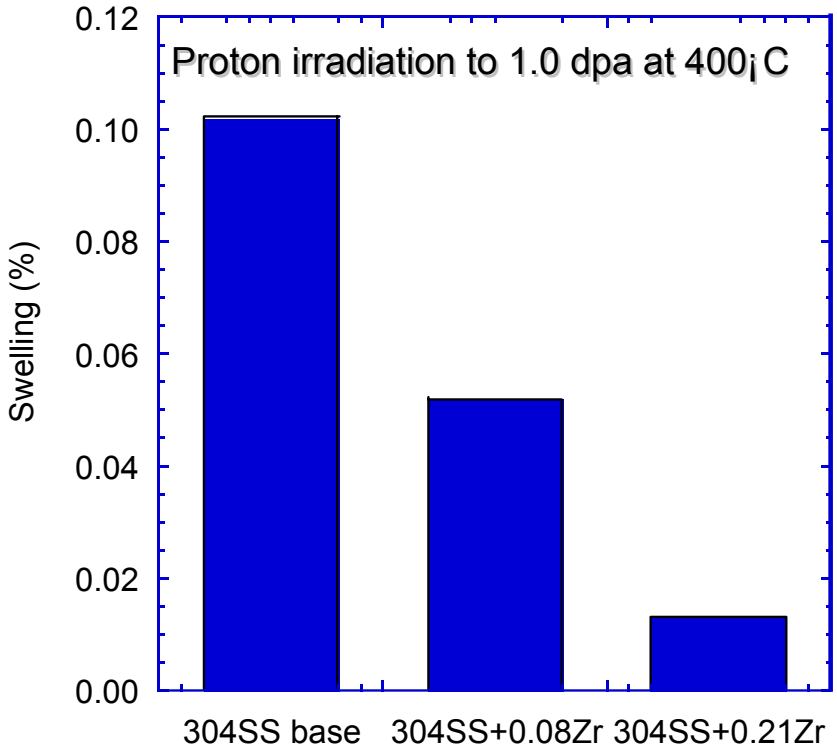

Figure 2 Increasing the Zr content in 304 stainless steel decreases the amount of void swelling.

Contributing Authors:

T. R. Allen, Argonne National Laboratory
J. I. Cole, Argonne National Laboratory.
R. Dropek, University of Michigan
J. Gan, Argonne National Laboratory
G. S. Was. University of Michigan

1.0 Introduction

Many nuclear reactor core structural components are made of austenitic stainless steel. These alloys are chosen because of their overall corrosion resistance and relative radiation stability. Although much effort has been expended on understanding the effect of radiation on stainless steels, there are still areas of concern for both light water reactors and other advanced reactor concepts. The areas of concern include environmental cracking and void swelling. Environmental cracking is anticipated to be a concern for advanced water-cooled and lead-cooled reactors. Cracking in difficult to repair components has the potential to significantly decrease plant availability. Void swelling is a concern in advanced reactors that operate at higher temperatures with extended component lifetimes. Reactor structural components with negligible swelling will be required. This project will use three techniques to provide insight into solving these reactor material problems: bulk composition engineering, grain boundary composition engineering, and grain boundary structural engineering.

Bulk composition engineering uses alterations to material composition to achieve superior performance. The bulk composition engineering studies in this work were comprised of three parts, all aimed at mitigating radiation damage. The first is to determine the effect of increasing bulk nickel concentration in an Fe-18Cr-9Ni alloy (corresponding to 304 stainless steel). The second is to determine the effect of adding molybdenum and phosphorous to an Fe-16Cr-13Ni alloy (corresponding to 316 stainless steel). The third is to add zirconium, an oversized alloy, to an Fe-18Cr-9Ni alloy (corresponding to 304 stainless steel).

The grain boundary composition engineering studies used various heat-treating and cooling methods to change the composition at grain boundaries prior to irradiation. The grain boundary structural engineering studies used various deformation and heat-treating methods to change the structure of grain boundaries prior to irradiation. In each case, the intent was to decrease the probability that the samples would fail along grain boundaries.

Samples were irradiated using 3.2 MeV protons at 400°C to either 0.5 or 1 displacement per atom (dpa). Following irradiation, samples were analyzed using a transmission electron

microscope (TEM). Swelling was characterized by measuring the void size distribution and density in the TEM samples. Radiation-induced grain boundary segregation was measured using a field emission gun scanning transmission electron microscope (FEG-STEM). Microhardness measurements were performed on alloys before and after irradiation to estimate the effect of irradiation on yield strength. Environmental cracking resistance was determined using constant extension rate mechanical tests in light water reactor chemistry at 288ºC.

This report describes material degradation in reactor structural materials, specifically void swelling and irradiation assisted stress corrosion cracking and the radiation-induced microstructural changes that make materials more susceptible to radiation damage. The three techniques used in this study to improve radiation tolerance are then described. The experimental procedure and results are then described and discussed.

This project was the joint effort of Argonne National Laboratory and the University of Michigan. The project required the combined efforts of both institutions and was a critical component to the graduate studies of a University of Michigan student.

2.0 Background

The research in this project aimed at improving radiation tolerance in austenitic stainless steel components. Two specific degradation mechanisms were addressed: void swelling and irradiation assisted stress corrosion cracking (IASCC). Three techniques aimed at improving radiation tolerance were researched: bulk composition engineering, grain boundary composition engineering, and grain boundary structural engineering

2.1 Materials Degradation in Reactor Structural Materials

Radiation can affect many mechanical and dimensional stability properties of structural components. Two of concerns to multiple advanced reactor designs are void swelling and IASCC (or more generally environmentally assisted intergranular cracking). Fundamental to these macroscopic degradation mechanisms are the associated radiation-induced changes to the microstructure and microchemistry of the material.

2.1.1 Void Swelling

Void swelling is the dramatic density decrease caused by the formation of small cavities in irradiated steel. An example of these voids is given in figure 2.1. An example of severe swelling is shown in figure 2.2. The practical consequences of excessive swelling are the limitation of component lifetime due to unacceptable changes in component geometry. Eliminating or delaying void swelling is important to plant reliability.

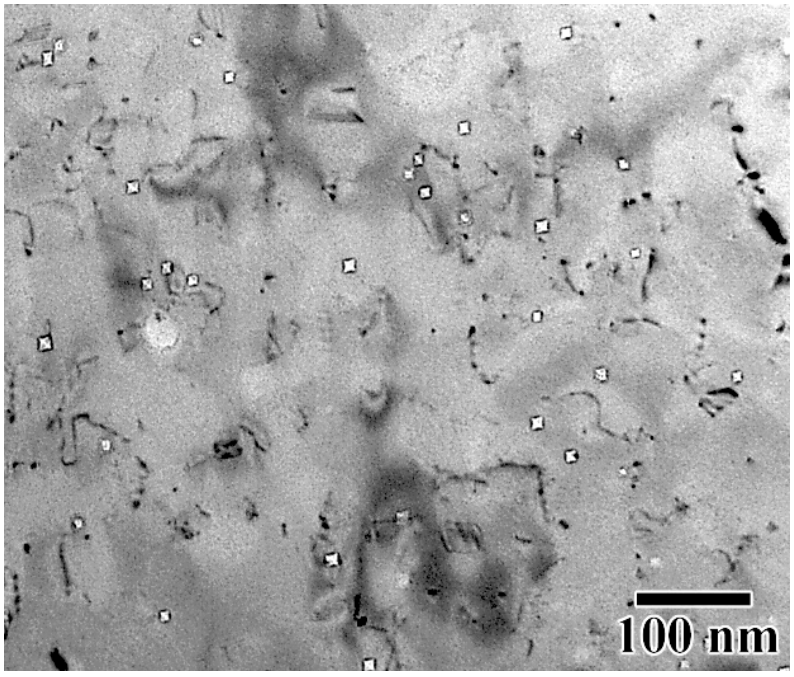

Figure 2.1 Voids in an austenitic stainless steel.

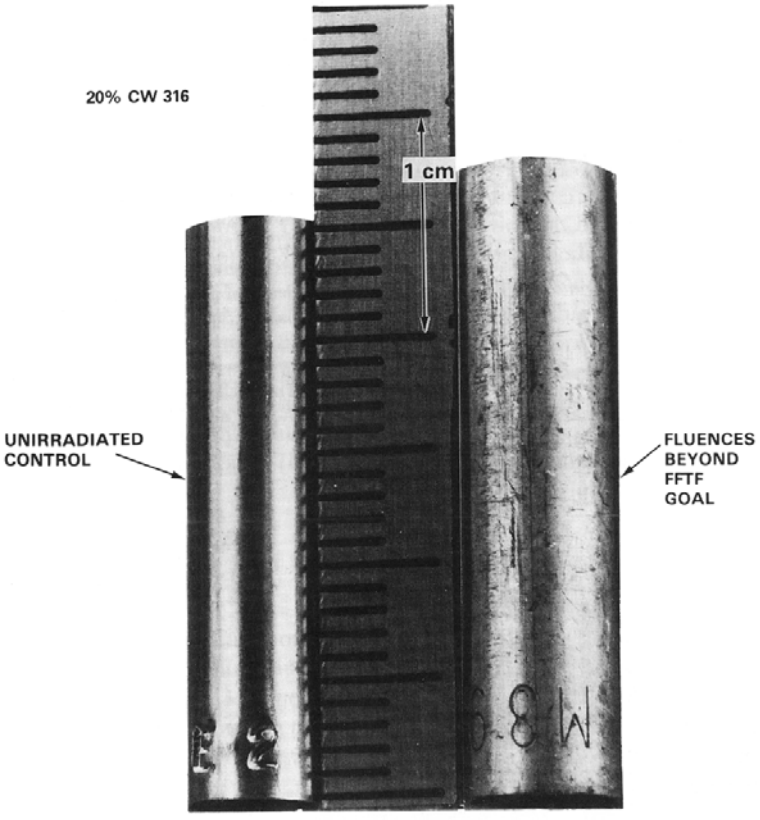

Figure 2.2 An example of extreme swelling in cold-worked 316 stainless steel [1].

2.1.2. Irradiation Assisted Stress Corrosion Cracking

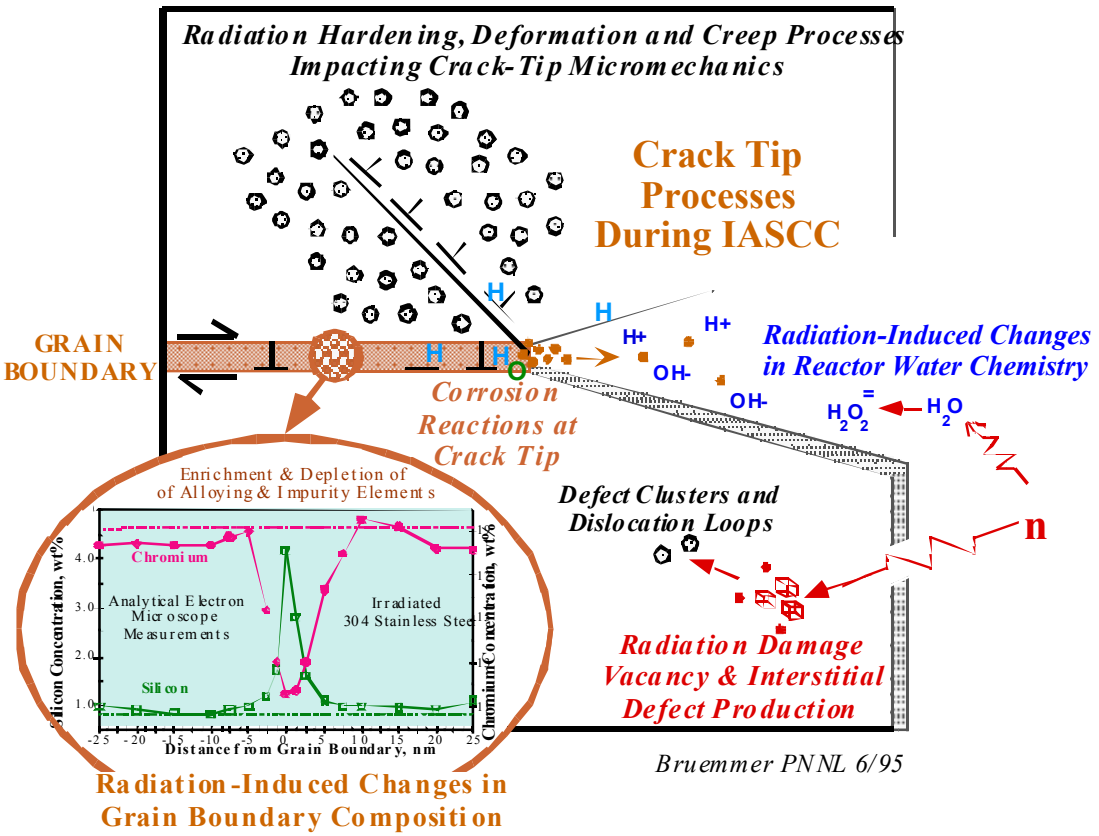

Figure 2.3 Schematic diagram of contributing factors to IASCC [2].

Irradiation assisted stress corrosion cracking is a stress corrosion cracking failure of irradiated material. IASCC is evidenced by cracking along grain boundaries. Three radiation-induced changes are believed to contribute to IASCC (figure 2.3). The first is electrolysis of water into radicals that increase the corrosive effect of reactor coolant. The second is hardening of the bulk material away from the grain boundaries, leaving the grain boundary as the weak portion of the material. The radiation hardening is caused by the development of voids (figure 2.1), dislocation loops (figure 2.4), and precipitate phases. The third potential contributor to IASCC is radiation-induced segregation (RIS). RIS causes the depletion of chromium at grain boundaries (figure 2.5). Since chromium is the alloying element that makes stainless steels corrosion resistant, the depletion of chromium at the grain boundary may make the boundary more susceptible to corrosion. The exact relevance of each contributing factor is not well understood, but techniques that eliminate radiation hardening or RIS should mitigate IASCC. Although IASCC is of

concern in water reactors, similar environmentally assisted cracking may occur in other reactor types. For instance, in lead-cooled reactors, intergranular cracking might also occur in irradiated components potentially weakened by nickel enrichment at grain boundaries, where nickel is soluble in lead or lead-bismuth eutectic.

Figure 2.4 Dislocation loops in an austenitic stainless steel.

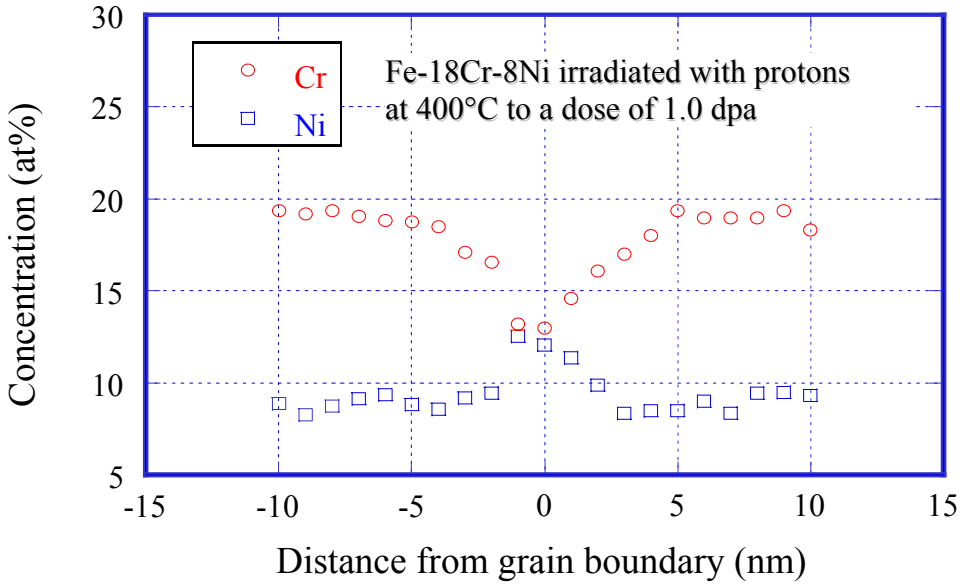

Figure 2.5 Radiation-induced segregation in an austenitic stainless steel.

2.2 Materials Processing to Mitigate Radiation Damage

Three different techniques were used in this work to improve radiation tolerance of austenitic stainless steels. The three techniques were bulk composition engineering, grain boundary composition engineering, and grain boundary structural engineering.

2.2.1 Bulk Compositional Engineering

Three different bulk composition techniques were studied. The first was to increase the bulk nickel concentration. Studies on model alloys also indicate increasing bulk nickel concentration decreases swelling [3]. The relative swelling and IASCC resistance of 304 and 316 stainless steel indicate increasing nickel as a means of improving radiation tolerance. Although there are a few compositional differences between 304 and 316, a major difference is bulk nickel content. 304 stainless steel contains between 8-10 wt. % while 316 stainless steel contains between 10 and 14 wt. %. Porter et al. [4] have shown that the swelling in 316 stainless steel is delayed to higher irradiation dose and that the difference lies in the void morphology. In 304, void number density saturates and these voids grow to large size causing the large swelling. In 316, the void size saturates forcing new voids to grow. The voids in 316 are thus smaller leading to less swelling. Although the difference in void morphology was hypothesized to be caused by microchemical segregation, no studies have been performed to correlate segregation and void morphology in austenitic alloys.

Bulk nickel increases may also reduce the susceptibility to IASCC. Tanaka et al., [5] compared the cracking response of 304 and 316 stainless steel in a slow strain rate stress corrosion cracking tests in water. The strain to crack initiation and the total strain are greater in the 316. The first bulk compositional technique was to compare the radiation response of three alloys: Fe-18Cr-9.5Ni-1.75Mn (corresponding to 304 stainless steel), Fe-16Cr-13Ni-1.25Mn (corresponding to 316 stainless steel), and Fe-18Cr-40Ni-1.25Mn (corresponding to 330 stainless steel). These alloys hold bulk chromium relatively constant while changing bulk nickel.

The second bulk composition engineering technique examined was the effect of the minor elements molybdenum and phosphorous on the performance of 316 stainless steel. The goal was to determine the contribution of these elements to the superior properties of 316 stainless steel relative to 304 stainless steel. As mentioned above, one major difference between the two alloys is the amount of bulk nickel. The second major difference is the addition of molybdenum. 316 stainless steel contains 2-3 wt. % molybdenum while 304 stainless steel has no molybdenum. In the second bulk engineering task, three alloys were examined: Fe-16Cr-13 Ni-1.25Mn, Fe-16Cr-13 Ni-1.25Mn +Mo, and Fe-16Cr-13 Ni-1.25Mn+Mo+P. Even though 304 and 316 both have phosphorous, increasing phosphorous has been shown to increase IASCC susceptibility in 316 stainless steel (figure 2.8). Some synergy between molybdenum and phosphorus could contribute to the superior performance of 316.

The third and final bulk composition technique was the addition of the oversized element Zr to 304 stainless steel. The addition of zirconium was chosen to test the hypothesis that an oversized element will act as a vacancy trap and prevent segregation and swelling by limiting point defect diffusion. Irradiations using high-energy electrons indicate the small amounts of zirconium will minimize segregation and swelling. Figures 2.6 and 2.7 [6] show that zirconium added to 316 stainless steel minimizes both grain boundary segregation and swelling. Understanding the microstructural basis for the apparent beneficial effect of zirconium and determining if zirconium additions mitigate IASCC was the basis for testing the zirconium-doped alloys. For these studies, three alloys were tested: Fe-18Cr-9.5Ni-1.75Mn, Fe-18Cr-9.5Ni-1.75Mn +0.04Zr, and Fe-18Cr-9.5Ni-1.75Mn +0.16Zr.

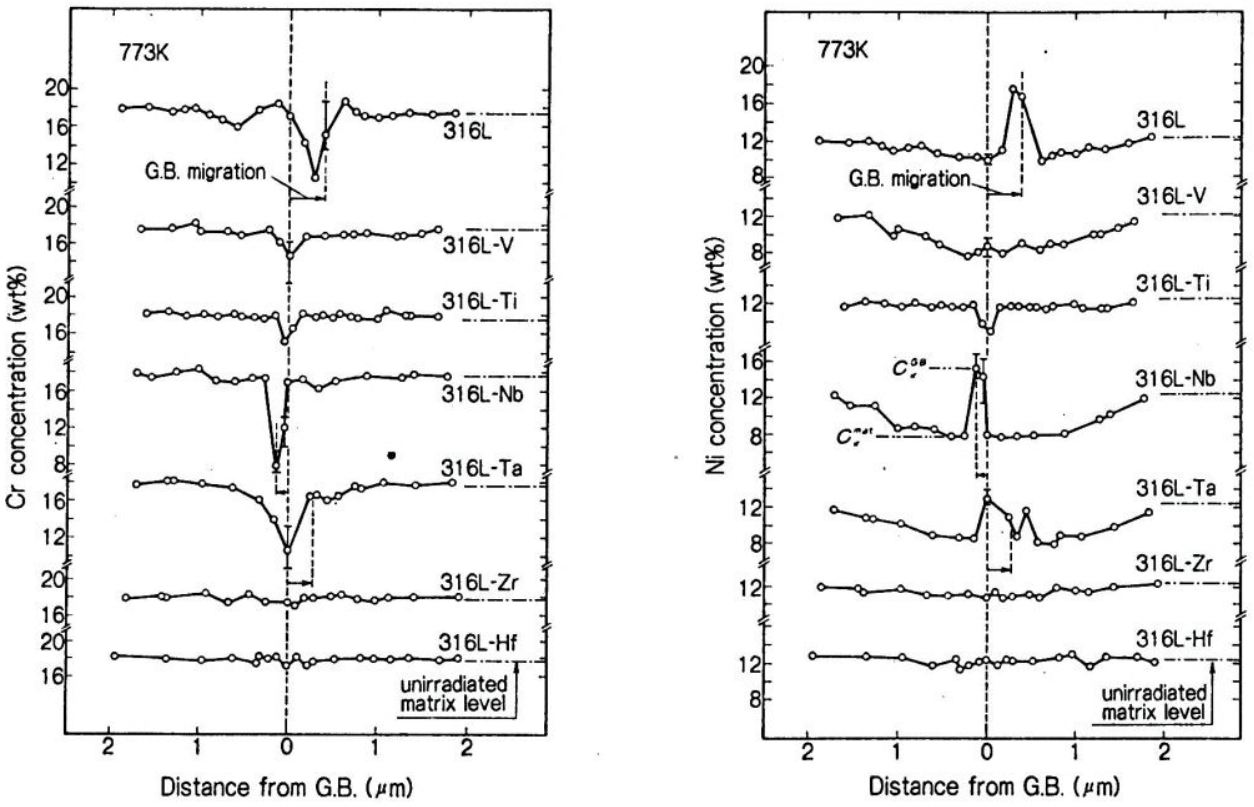

Figure 2.6 Effect of zirconium RIS in 316 base alloys [6].

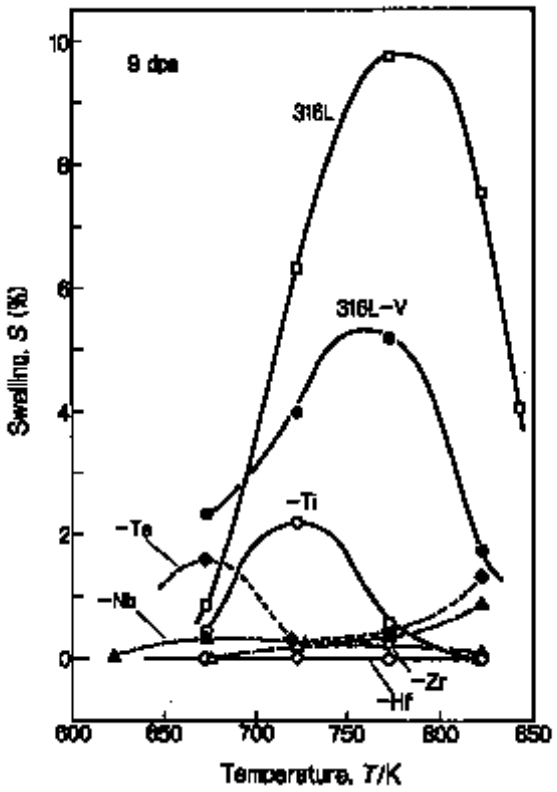

Figure 2.7 Effect of zirconium swelling in 316 base alloys [6].

2.2.2 Grain Boundary Compositional Engineering

The intent of grain boundary engineering is to create grain boundaries that prevent environmental cracking or extend the crack initiation time beyond reactor lifetimes. Grain boundary composition can be controlled by three methods: adding an element that depletes more strongly than chromium, enhancing the enrichment of chromium at the grain boundary prior to irradiation, or shutting down the segregation process by limiting the flux of point defects to the boundary. For this project, appropriate heat treatments will be determined to set the grain boundary composition prior to irradiation. Three alloys were tested for these studies: Fe-16Cr-13 Ni-1.25Mn, Fe-16Cr-13 Ni+Mo-1.25Mn, and Fe-16Cr-13 Ni-1.25Mn+Mo+P. The goal is to find annealing temperature and cooling rate combinations that maximize the grain boundary chromium prior to irradiation. If chromium depletion is critical to IASCC then maximizing the grain boundary chromium concentration prior to irradiation could delay the onset of IASCC.

2.2.3 Grain Boundary Structural Engineering

In grain boundary *structure* engineering, a series of thermomechanical treatments will be used to develop a material with large numbers of low angle grain boundaries. These boundaries are expected to exhibit less grain boundary chromium depletion and thus be less susceptible to environmental cracking. If chromium depletion is critical to IASCC then by changing the grain boundary structure to reduce the grain boundary chromium depletion could delay the onset of IASCC. Additionally, optimizing the fraction of low angle boundaries is expected to decrease the creep by limiting the mobility of extrinsic grain boundary dislocations in the special boundaries. If grain boundary deformation processes are critical to IASCC, then these treatments should improve resistance. In this project, two alloys were studied: Fe-18Cr-9.5Ni-1.75Mn (corresponding to 304 stainless steel) and Fe-16Cr-13Ni-1.25Mn (corresponding to 316 stainless steel). Two specific goals were targeted in studying these alloys. First to help understand the different cracking resistance between 304 and 316 stainless steel and second to understand the effect of grain boundary structure modifications in the two most common reactor materials.

2.3 Experimental Program Design

The five subsets of the test matrix are presented in Table 2.1. The overall program is shown in figure 2.8. Five separate experimental tracks were followed, three bulk composition engineering tasks, one grain boundary composition engineering task, and one grain boundary structure engineering task. Although each of the five subsets had a specific goal, the possibility was anticipated that some of the separate improvements could be combined. For instance, the addition of bulk zirconium and the grain boundary enrichment of chromium together might make improvements that neither task could individually.

The alloy compositions are listed in Table 2.2.

Table 2.1 Test matrix

Processing Technique	Alloys
Bulk Composition Engineering (Bulk Nickel Series)	
	Fe-18Cr - 8Ni-1.25Mn
	Fe-16Cr-13Ni-1.25Mn
	Fe-18Cr-40Ni-1.25Mn
Bulk Composition Engineering (316 series)	
	Fe-16Cr-13Ni-1.25Mn
	Fe-16Cr-13Ni-1.25Mn+Mo
	Fe-16Cr-13Ni-1.25Mn+Mo+P
Bulk Composition Engineering (Zirconium series)	
	Fe-18Cr-9.5Ni-1.75Mn
	Fe-18Cr-9.5Ni-1.75Mn+0.04Zr
	Fe-18Cr-9.5Ni-1.75Mn+0.16Zr
Grain Boundary Composition Engineering (Cr pre-enrichment of 316 series)	
	Fe-16Cr-13Ni-1.25Mn
	Fe-16Cr-13Ni-1.25Mn+Mo
	Fe-16Cr-13Ni-1.25Mn+Mo+P
Grain Boundary Structural Engineering (CSL enhancement of "base" 304 and 316)	
	Fe-18Cr-9.5Ni-1.75Mn
	Fe-16Cr -13Ni-1.25Mn

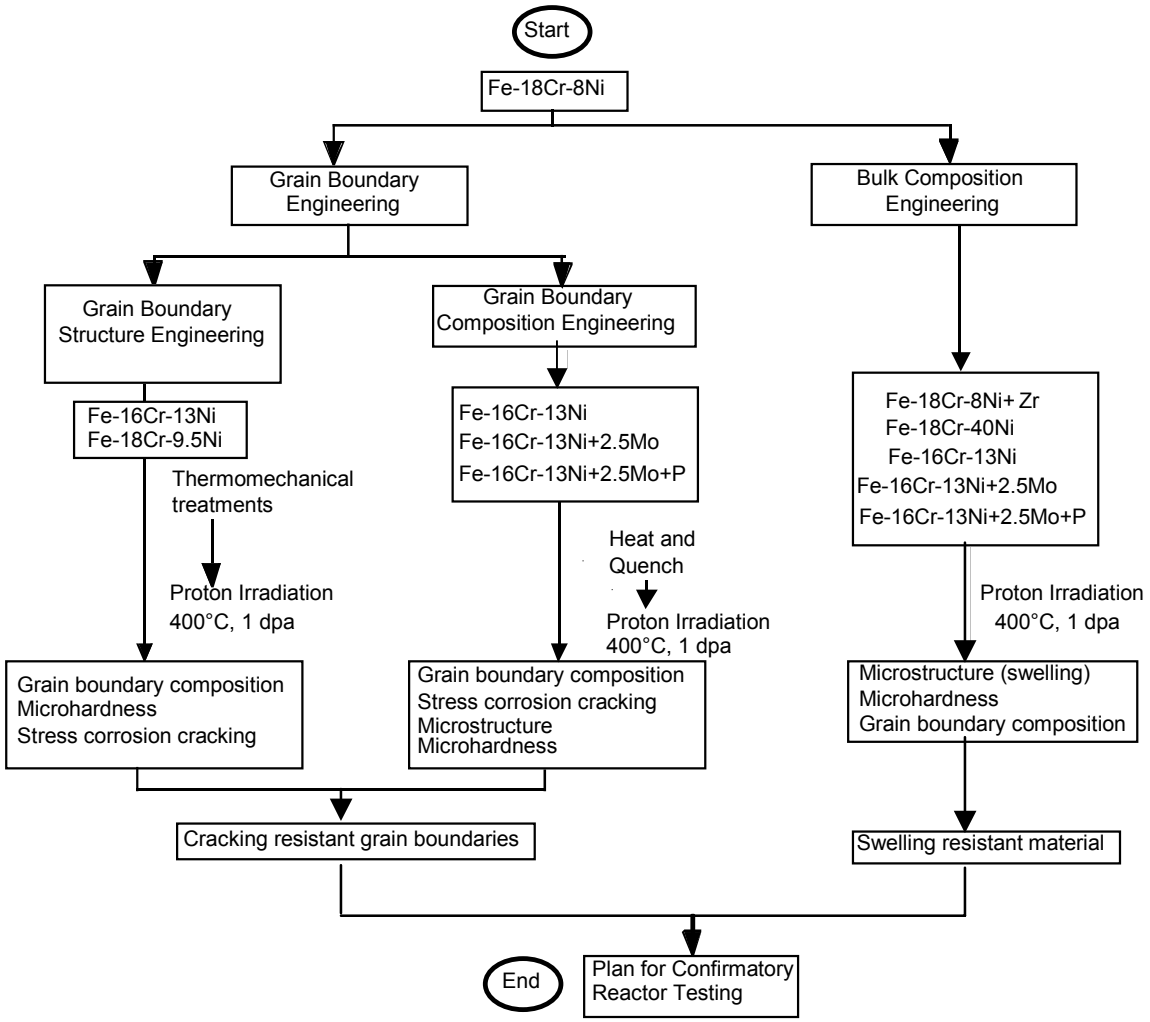

Figure 2. 8 Experimental plan.

Table 2.2 Alloy composition (wt%)

Alloy Designation	Fe	Cr	Ni	Mn	Mo	P	Zr	C
Fe-18 Cr-8 Ni-1.25Mn	72.4	18.1	8.4	1.1	<0.01	<0.01	<0.01	0.01
Fe-18 Cr-9.5Ni-1.75Mn	70.0	18.6	9.7	1.74	<0.01	<0.01	<0.01	<0.01
Fe-16Cr-13Ni-1.25Mn	70.3	15.6	12.9	1.2	<0.01	<0.01	<0.01	0.01
Fe-18 Cr-40 Ni-1.25Mn	40.0	18.1	40.7	1.2	<0.01	<0.01	<0.01	0.01
Fe-16Cr-13Ni-1.25Mn+Mo	68.4	15.4	13.2	1.2	1.85	<0.01	<0.01	0.01
Fe-16Cr-13Ni-1.25Mn+Mo+P	68.5	15.4	13.0	1.2	1.83	0.05	<0.01	0.01
Fe-18Cr-9.5Ni-1.75Mn-0.04Zr	69.1	19.1	10.0	1.74	<0.01	<0.01	0.04	0.02
Fe-18Cr-9.5Ni-1.75Mn-0.16Zr	70.3	18.2	9.6	1.75	<0.01	<0.01	0.16	<0.01

2.4 Proton Irradiation

Proton irradiation has several significant advantages over neutron irradiation in studying structural materials degradation: a) it is significantly less expensive than neutron irradiation; b) the irradiation time is substantially shorter and c) sample activation is negligible so that extensive characterization is more straightforward. All of these attributes combine to give proton irradiation an advantage over neutron irradiation in that experimental iterations (irradiation – characterization – testing) can be conducted multiple times in the course of a year, greatly aiding the process of mechanism identification. Since the displacement rate and the displacement cascade characteristics of proton irradiation differ from those of neutron irradiation in reactor, it is important to establish that the former produces the same changes in the material studied. As described below, proton irradiation produces changes in microstructure, hardness, grain-boundary segregation, and SCC behavior that are similar to those produced by neutron irradiation in light water reactors.

The penetration depth of 3.2 MeV protons in stainless steel is 40 μm and creates fairly uniform damage over a region of 35 μm. Since the thickness of the uniform-damage region includes several grain diameters, we are able to study the effect of radiation-induced changes on intergranular cracking. The displacement rate during a 3.2 MeV proton irradiation is 10^2 to 10^3 times greater than for typical in-core irradiation of light water reactors. Thus, the balance between energetic displacement and thermal processes is very different for the two particle types. By conducting proton irradiations at higher temperatures than exist in core, a balance similar to that in neutron irradiation can be achieved [7]. The highlights of our results and other researchers' results which are given below demonstrate that such an approach is successful.

In addition to increasing the density of network dislocations, irradiation creates a high density of dislocation loops and "black dots", neither of which are observed in cold-worked solids. This difference is important since dislocation loops cause a localization of deformation into channels. Ref. [7] contains a comparison of the loop, network and "black dot" densities and loop diameters for 300-series austenitic stainless steel neutron irradiated at 288 °C to 1-10 dpa, or irradiated with

3.4 MeV protons to 1 dpa, and shows that the structural damage produced by reactor irradiations is reproduced by our proton irradiations. A more specific comparison is shown in Fig. 2.9, which plots the dislocation loop size distributions for proton- and neutron-irradiated 316SS from the same heat. Note the excellent correlation between 1 dpa proton irradiation data and the 1.1 dpa neutron data.

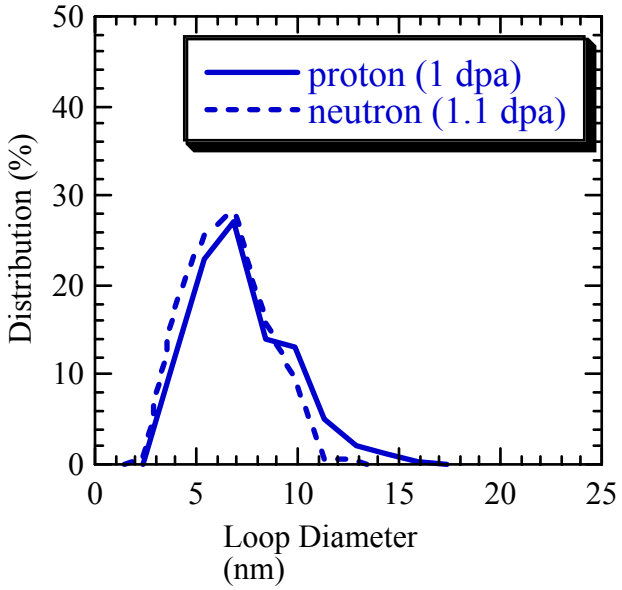

Figure 2. 9 Dislocation loop size distribution in 316SS irradiated with neutrons at 275°C between 0.8 and 3.4 x 10^{21} n/cm^2 (1 - 5 dpa), and with protons at 360°C to 1 dpa.

The most pronounced effect of the dislocation microstructure is irradiation hardening. Fig. 2.10 shows the hardening (represented by the yield stress) as a function of dose for 3.2 MeV proton irradiations in comparison to the database on 300 series stainless steels, irradiated and tested around 300°C. The agreement with neutron data is excellent, and is consistent with that expected from the microstructure results.

A comparison of grain-boundary segregation data is more challenging because of the large scatter inherent to their measurements. Figure 2.11 shows a compilation of grain-boundary Cr concentration measurements by FEG-STEM [8] along with data from our proton irradiations (shaded symbols). As shown, the agreement is excellent over a range of doses and alloys. A comparison of typical concentration profiles measured by FEG-STEM in proton- and neutron

irradiated 316SS is shown in Fig. 2.12. These data have been obtained for a 316 stainless steel heat irradiated with protons to 1 dpa at 360°C [9]. Comparison to neutron irradiation (of the same heat) in-core at 275°C to 1.4 dpa reveals remarkable agreement in both the magnitude and spatial extent of segregation of major alloying elements and impurities, and even the fine detail of the "W" shaped chromium profiles that have been discovered in irradiated stainless steels.

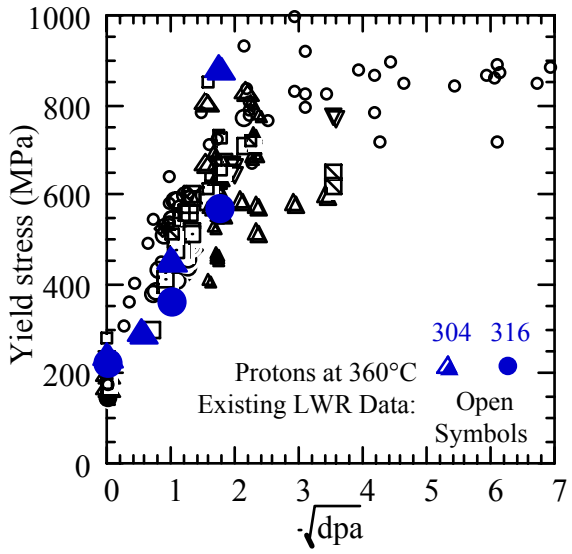

Figure 2.10 Yield strength of irradiated 300 series stainless steels irradiated (in reactor) and tested at about 300°C and compared to values from proton irradiation and compared to results from neutron irradiation.

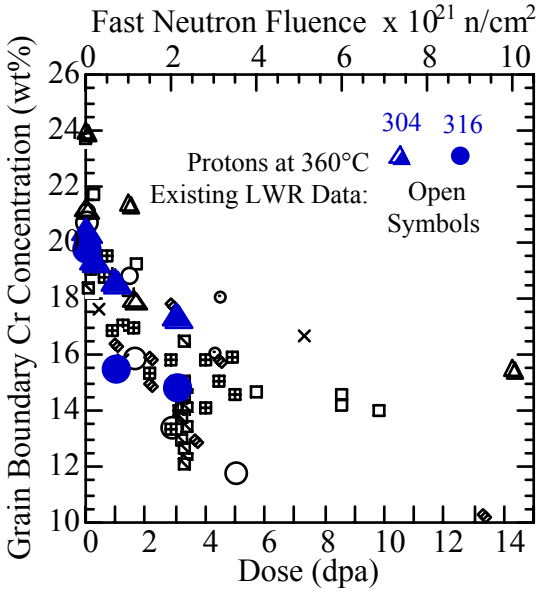

Figure 2.11 Grain boundary chromium concentration as a function of dose for 304 and 316SS irradiated with 3.2 MeV protons.

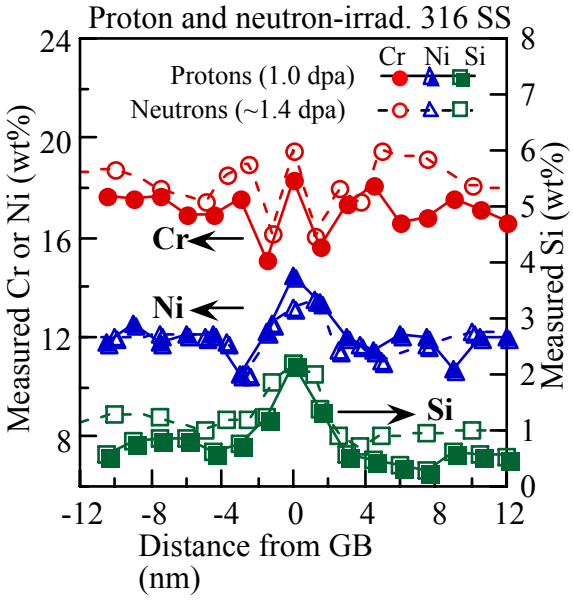

Figure 2 12 Comparison of Cr, Ni and Si concentration profiles at the grain boundary of 316 SS irradiated with neutrons at 275°C to 1.4 dpa (closed symbols) and with protons at 360°C to 1.0 dpa (open symbols).

Finally, we have consistently observed that proton irradiation, under the same conditions as neutron irradiation, causes IASCC susceptibility in austenitic stainless steel [10]. Figure 2.13 shows the results of constant extension rate tests in BWR water conditions of both a 304 and a 316 alloy that has been irradiated with 3.2 MeV protons and separately, with neutrons in-core. Note that the threshold dose for cracking is identical for the 304 alloy and that through 3.0 dpa, no cracking has been observed in the proton irradiated 316 alloy, consistent with the neutron results. Figure 2.14 shows that cracking in proton-irradiated alloys agrees with SCC results from neutron irradiation experiments which show that the higher nickel austenitic alloys are more resistant to IASCC [11].

Thus, proton irradiation is capable of creating similar chemical and structural changes as neutron irradiation, and produces the same sensitivity to SCC as does neutron irradiation. Hence, it is a well-developed technique for producing and studying the effects of neutron irradiation in reactor core materials.

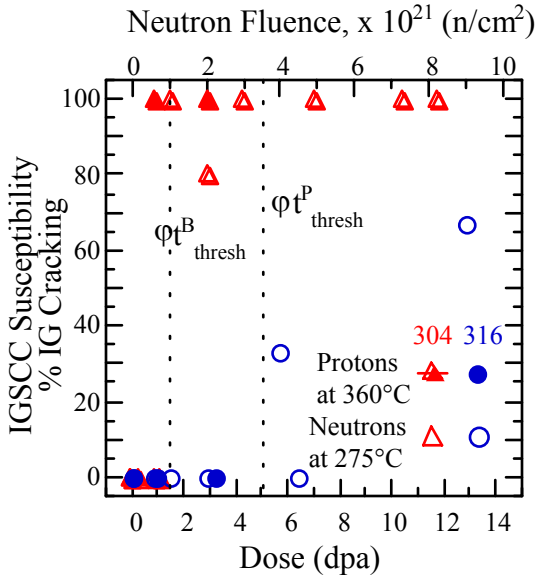

Figure 2.13 IASCC susceptibility of 304 and 316 stainless steel irradiated in reactor or with protons and tested in BWR water in constant extension rate until failure. Note that the threshold fluence is exactly the same for the 304 alloy and agrees with 316 for the data taken so far.

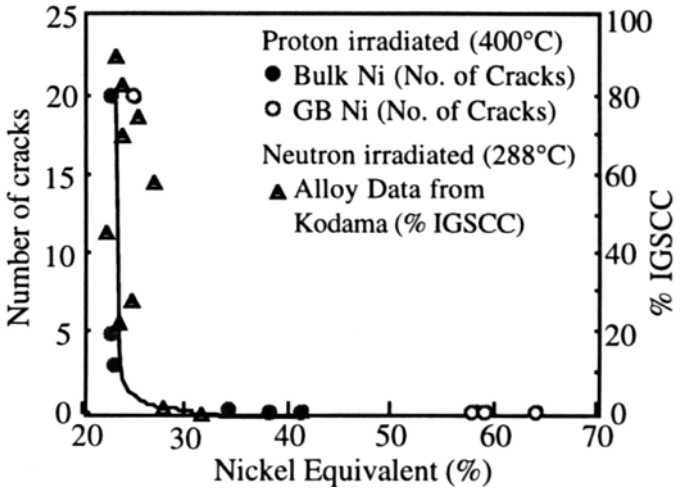

Figure 2.14 Effect of nickel equivalent on the IASCC susceptibility of several austenitic alloys from the study of Kodama [11]. The results from proton irradiation are plotted for comparison.

2.5 Limitation of Test Plan

For the test program carried out in this research project, each processing condition was only tested at a single irradiation temperature and dose. Although this does provide information as to the success of a specific technique, the success may be better or worse for different irradiation conditions. As an example, the grain boundary segregation for three different alloys is plotted in figure 2.15. In this example, each alloy has similar bulk chromium concentration, but the nickel concentration varies significantly. At low dose, the alloys with higher bulk nickel concentration have greater grain boundary chromium depletion. If the analysis stopped at low dose, the conclusion would be that higher bulk nickel would make an alloy more susceptible to IASCC (to the extent that IASCC correlates with chromium depletion). At higher dose, the alloy with the lower bulk nickel concentration has greater chromium depletion. At high dose, the conclusion would be that higher bulk nickel would make an alloy less susceptible to IASCC. Success of a particular technique in this study is limited to one specific irradiation condition and justifies an expanded test matrix.

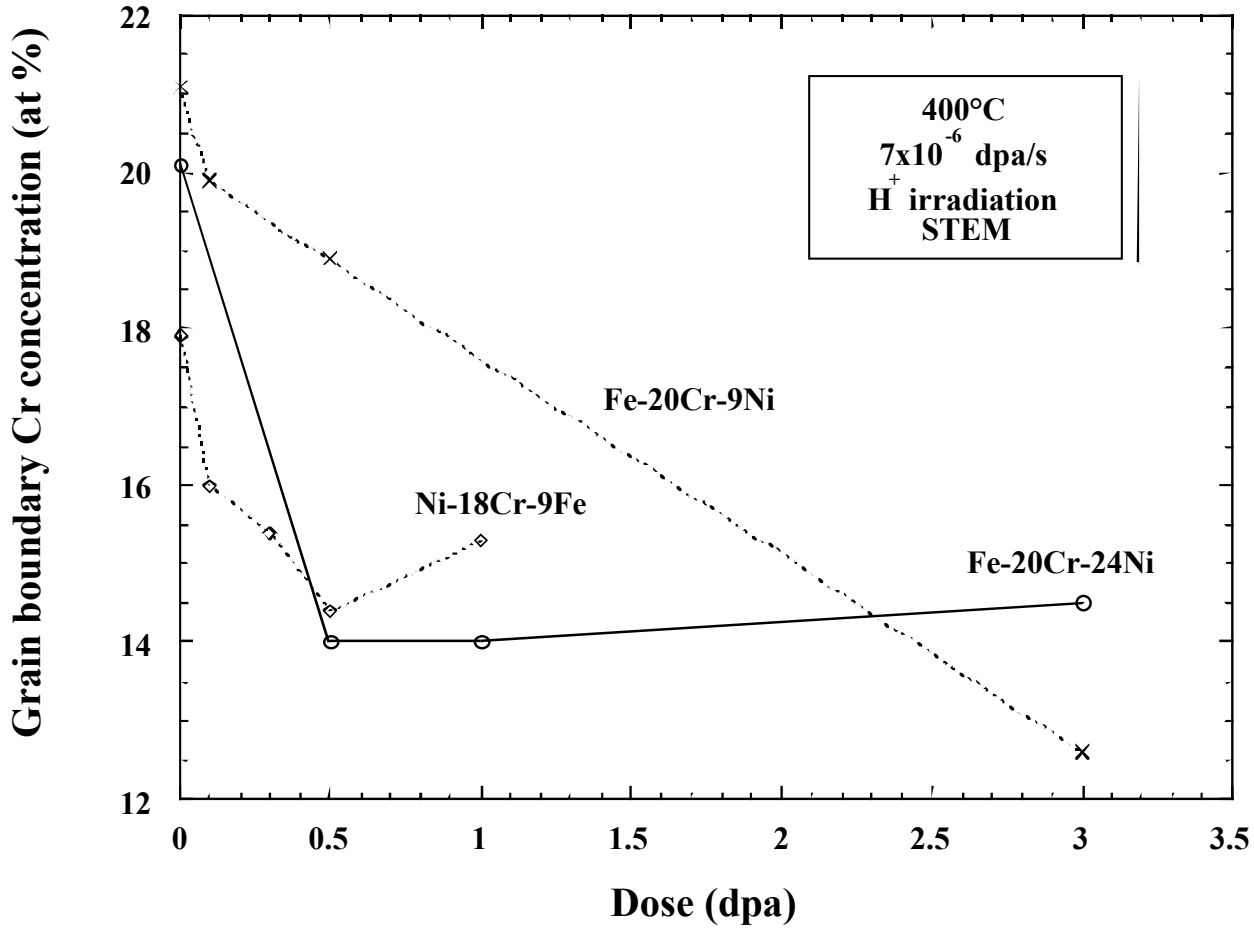

Figure 2.15 Effect of dose rate on radiation-induced segregation

3.0 Experiment

3.1 Material Preparation

All the alloys used in this project were made by General Electric Global Research in Schenectady, NY. The as-received materials were solution annealed at 1200°C for one hour and quenched in water. Each alloy was cold-worked to a 66% thickness reduction by cold-rolling. Samples of TEM coupons or SCC bars were then fabricated using electrical discharge machining (EDM). Samples for bulk composition engineering underwent a recrystallization anneal to obtain an average grain size of around 20 microns. Twenty-micron grains were desired because the range of damage in the 3.2 MeV proton beam used to irradiate samples is approximately forty microns. Twenty-micron grains would allow an average damage zone depth covering two grains (see figure 3.1). For grain boundary engineering studies, after the 66% thickness reduction by cold rolling, samples underwent different thermal mechanical treatments to achieve the Cr pre-enrichment at grain boundaries or to enhance the fraction of CSL boundaries. The details of material preparation for grain boundary engineering studies will be provided later in discussion.

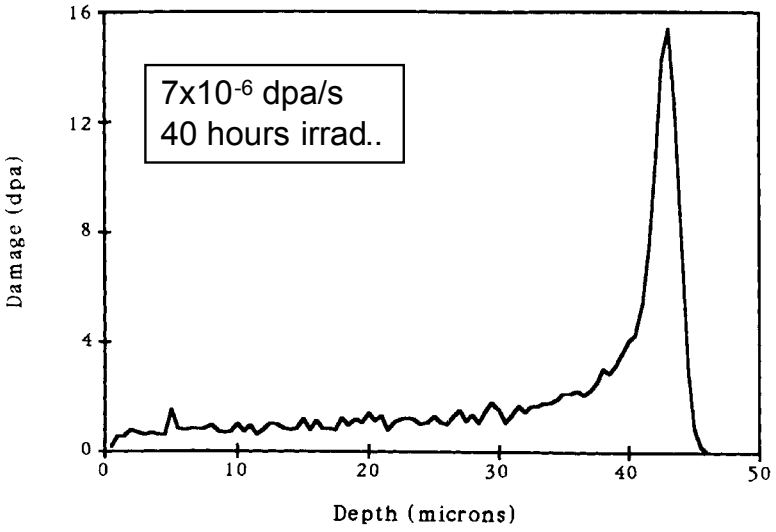

Figure 3.1 Displacement rate profile for 3.4 MeV protons in stainless steel as calculated by the Monte Carlo program TRIM 90.

3.2 Proton Irradiation

Sample irradiations were performed using the General Ionex Tandetron accelerator at the Michigan Ion Beam Laboratory. Irradiations were conducted using 3.2MeV protons at a dose rate of approximately $8x10^{-6}$ dpa/s. The samples were irradiated at 400°C to a final dose of 0.5 or 1 dpa. Details of the sample irradiation procedure can be found in reference [12].

3.3 Orientation Imaging Microscopy

For grain boundary structural engineering studies, orientation imaging microscopy maps were then acquired in a Philips XL30FEG SEM equipped with OIM system (OIM, TSL Inc., Draper, UT). This system allows for automatic recognition and indexing of adjacent grains, thereby providing for the characterization of several hundred grain boundaries in a single session. The characterized boundaries were classified according to the coincident site lattice model as either low angle boundaries (LAB, $\Sigma = 1$), coincident site lattice boundaries (CSLB, $1< \Sigma \leq 37$) or high angle boundaries (HAB, $\Sigma > 37$). The CSL value Σ represents the reciprocal density of coincident atomic sites between two crystals, and the criterion for deciding a CSL designation was Brandon's criterion (Brandon 1966) with a maximum allowable deviation from exact coincidence $\delta\theta = 15° \, S^{-0.5}$.

3.4 Microhardness

Microhardness is used to estimate changes in mechanical properties during irradiation. Microhardness was measured on each of the alloys both prior to and after irradiation. Vickers hardness was measured using a Vickers Microhardness Tester (Micromet-II). A total of 30 to 50 indents at a load of 25 g were applied on the TEM bar in both the irradiated region and the unirradiated region. Since proton irradiation produces a fairly uniform damage layer over the

first 35μm, a low load of 25g with load time of 20 seconds was applied to ensure that the unirradiated material below the damaged layer was not being sampled. The center to center spacing of indents is approximately 100μm, so that specimen deformation from an indent does not affect results of subsequent indentations.

The hardness change can be related to an increase in yield strength using the relation

$$\Delta\sigma_y = K\Delta H_v.$$

When yield strength is in MPa and hardness is measured in HV (kg/mm^2), the conversion factor K for alloys corresponding to 304 stainless steel (Fe-18Cr-8Ni) is 3.48 and the conversion factor K for alloys corresponding to 316 stainless steel (Fe-16Cr-13Ni) is 3.27 [13]. Since a correlation factor has not been identified for the 40 at % Ni alloy, the 3.27 factor for 316 stainless steel was used.

3.5 Transmission Electron Microscopy

All changes in bulk properties are determined by changes to the microstructure. Void and dislocation loop distributions were measured using a JEOL 2010 TEM. Analysis was carried out in the TEM operating at an accelerating voltage of 200 kV. Sample thickness for cavity density measurements was determined using convergent beam electron diffraction (CBED) at **g**=311. The density and size of voids were measured from bright field images with electron beam condition away from any strong diffraction conditions. The density and size of Frank loops were measured from the rel-rod dark field images in which only faulted loops are present [14-15]. Each TEM sample was examined to determine if there were any precipitates before and after irradiation.

3.5 Scanning Transmission Electron Microscopy with Energy Dispersive X-Ray Spectroscopy (STEM/EDS)

Grain boundary compositions were measured using scanning transmission electron microscopy with energy dispersive x-ray spectroscopy (STEM/EDS). The STEM/EDS was performed at Oak Ridge National Laboratory on a Phillips CM200 equipped with a field emission gun source. An accelerating voltage of 200 kV was used. STEM/EDS measurements were performed at the grain boundary and at increments of 1.0 nm away from the boundary to give compositional profiles. The incident probe thickness was approximately 1.4 nm (full width, tenth maximum). The sample is tilted towards the x-ray detector and each grain boundary analyzed is aligned such that the boundary is "edge-on" (parallel to the electron beam). This placement ensures that the measured x-ray intensity has equal contributions from both sides of the boundary. All profiles were performed at a magnification of 1,000,000 times.

Once an EDS spectrum (intensity of the K_α peak for each element versus energy) has been gathered, the concentration is calculated from the relative intensities of each element. For the alloys of this study, x-ray intensities were collected for the K_α peaks of Fe (7.114keV), Cr (5.989keV), and Ni (8.333keV). No attempt was made to extract data from the Mn K_α peak. To ensure the measured x-ray intensities are representative of only the sample and not the background of the microscope, a "hole-count" spectrum is subtracted from the measured intensities prior to calculating the concentrations. A "hole-count" is performed by placing the electron probe in the sample perforation such that the probe travels through without interacting with the sample.

The ratio of the concentration of atom A to atom B is proportional to the ratio of the measured intensities, with the proportionality constant known as the k-factor:

$$\frac{C_A}{C_B} = k_{AB}\frac{I_A}{I_B}$$

Similarly, the ratio of the concentration of atom B to atom C is proportional to the ratio of the measured intensities:

$$\frac{C_B}{C_C} = k_{BC}\frac{I_B}{I_C}$$

Assuming that

$$C_A + C_B + C_C = \mathbf{1}$$

(that no other elements exist), the concentrations are calculated by simultaneously solving the three above equations. To calculate the k-factors, concentrations in the bulk of the material, away from the grain boundary segregation, are measured and k-factors are calculated using an independent measurement of the bulk composition. The k-factors used in this study were calculated by Busby for 304 and 316 stainless steel using the Phillips CM200 [16].

3.6 Stress Corrosion Cracking Testing

Stress corrosion cracking (SCC) resistance was estimated by performing constant extension rate tensile tests in simulated BWR normal water chemistry (NWC). Samples were strained at a rate of $3x10^{-7}$ s^{-1} in a multi-sample CERT system that strains four samples simultaneously. Independent load-displacement curves were collected for each sample and converted to stress-strain curves. Tests were conducted at 288°C in water containing 2 ppm oxygen and a conductivity of 0.2 μS/cm. The stress-strain characteristics are measured (figure 3.2) and relative SCC resistance is determined by the average crack length per unit of strain.

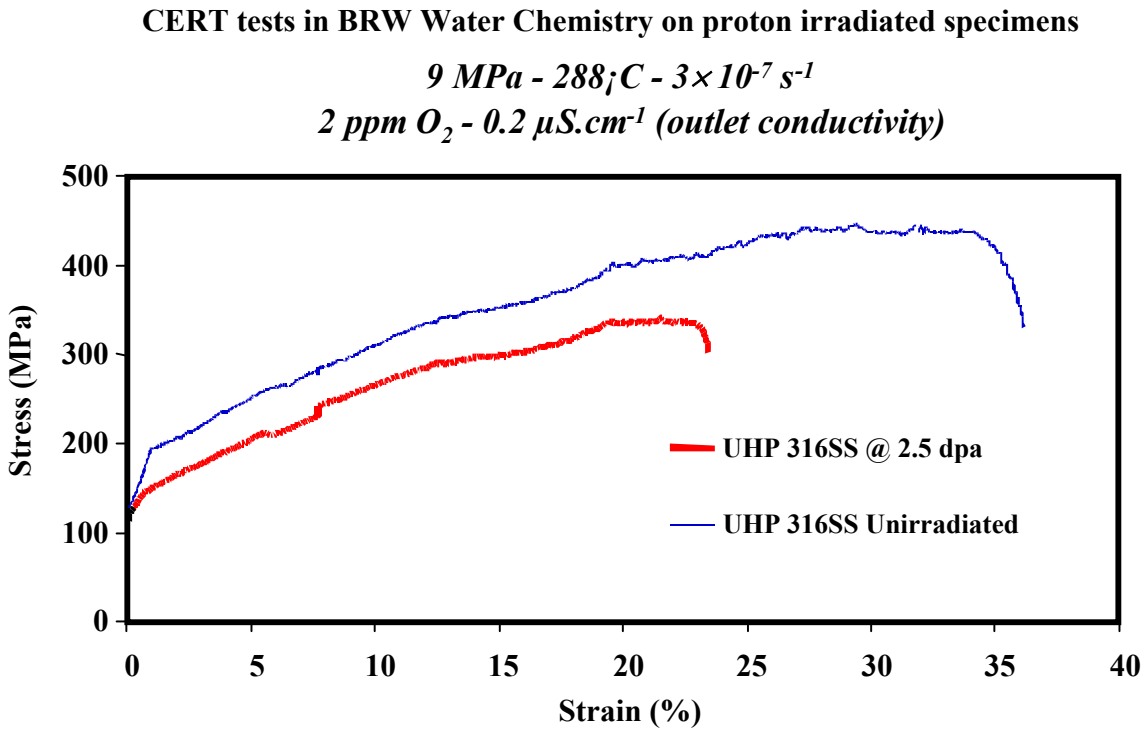

Figure 3.2 Example of a stress-strain curve from a stress corrosion cracking test.

4.0 Results and Discussion

4.1. Bulk Composition Engineering

Three different bulk composition engineering techniques were examined: increasing bulk nickel concentration, adding minor elements, and adding an oversized solute. For each, the hardening, swelling and IASCC response is discussed, along with the associated microstructural changes.

4.1.1 Effect of Increasing Ni in a 304 Base Alloy

Increasing the bulk nickel concentration caused an increase hardening. Figure 4.1 shows that as the bulk nickel increases from 8 to 40 wt. %, the change in hardness during irradiation increases. Because hardness and yield strength are related, increasing bulk nickel concentration leads to correspondingly greater increases in yield strength during irradiation. For austenitic steels, the increase in yield strength due to irradiation corresponds to a decrease in ductility [1]. Therefore, increasing the bulk nickel concentration is a detriment to radiation tolerance.

Increasing the bulk nickel concentration caused a decrease in swelling. Figure 4.2 shows that as the bulk nickel increases from 8 to 40 wt. %, the swelling during irradiation decreases significantly. The swelling at 0,5 dpa is a factor of 5 smaller in the 40 wt. % nickel alloy than in the 8 wt. % nickel alloy. As swelling can be a life limiting effect in austenitic stainless steels, the addition of nickel improves radiation tolerance.

The irradiation-induced microstructural changes as a function of bulk nickel concentration can be seen in figure 4.3. The density of both the voids and dislocation loops decreases as bulk nickel increases. There is not a consistent trend of the void or dislocation size with bulk nickel concentration. The decrease in swelling with increasing bulk nickel concentration is caused by the decrease in void density. Increasing bulk nickel makes nucleation of voids more difficult. This could be caused by a decrease of available point defects or difficulty in reaching the critical size for a void to grow.

The changes in grain boundary composition as a function of bulk nickel concentration are shown in figure 4.4. As the bulk nickel concentration increases, the grain boundary chromium depletion and nickel enrichment both increase. The segregation in the 40 wt. % nickel alloy is significantly greater than in the lower nickel materials. The increase in segregation that occurs at voids is expected to be similar to that at grain boundaries. Surrounding voids with a shell of slower diffusing nickel atoms is believed to inhibit the growth of voids to the critical size [16].

Although no SCC tests were completed for the bulk nickel series, the results of the hardening and grain boundary segregation can be examined for potential resistance to IASCC. IASCC is believed to be more likely in those materials with the greatest chromium depletion and the greatest yield strength. For the bulk nickel series, the higher nickel alloys have greater chromium depletion and greater hardening. The 40 wt. % nickel alloy had a slightly higher yield strength at 0.5 dpa. From these results, the higher nickel alloys would be expected to be more susceptible to IASCC. On the contrary, Cookson et al. found that increasing nickel concentration decreases IASCC susceptibility and as mentioned earlier, 316 (with a higher nickel concentration) is less susceptible. A potential explanation is that increasing bulk Ni increases the stacking fault energy, reducing the probability of channeling-type deformation and the associated stress concentrations at grain boundaries. The likely explanation for the discrepancy between hardening and segregation at 0.5 dpa and known IASCC resistance is the time dependence of the radiation damage as explained in section 2.5. At 0.5 dpa, the lower nickel alloys, with the slower developing microstructure, have not yet accumulated a susceptible microstructure.

Even though increasing bulk nickel improves swelling resistance, the increased hardening indicates poor high dose radiation response and no further testing of the bulk nickel series is recommended.

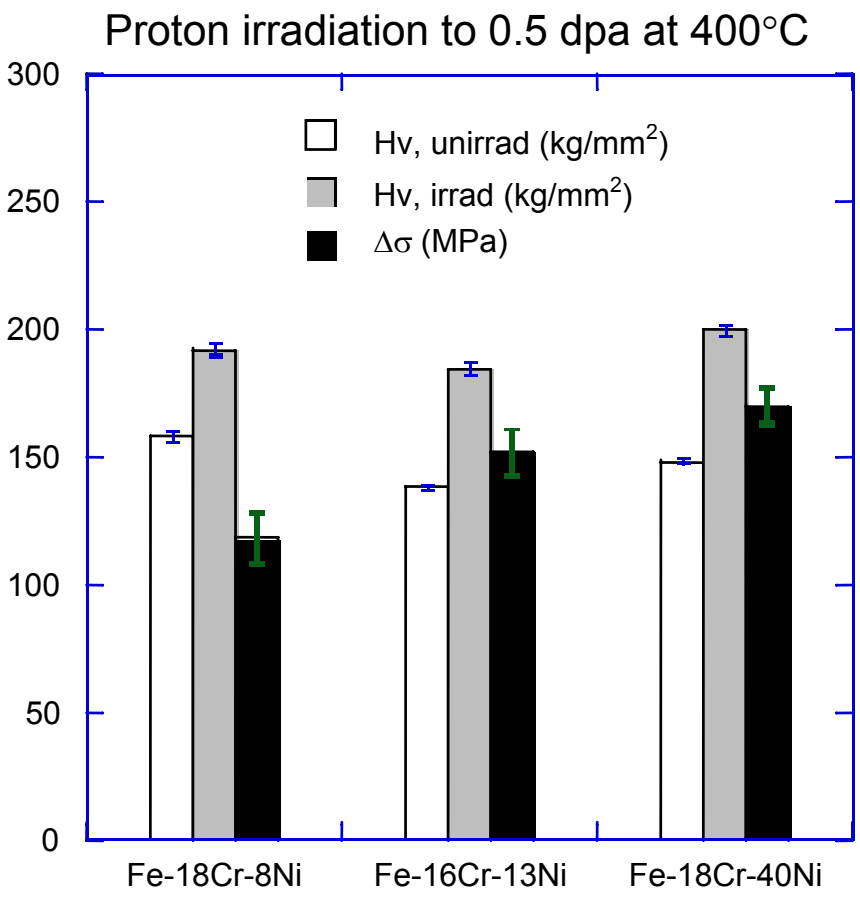

Figure 4.1 Hardness increase with increasing bulk nickel concentration, the error bars indicating the standard deviation of the mean for the measurements.

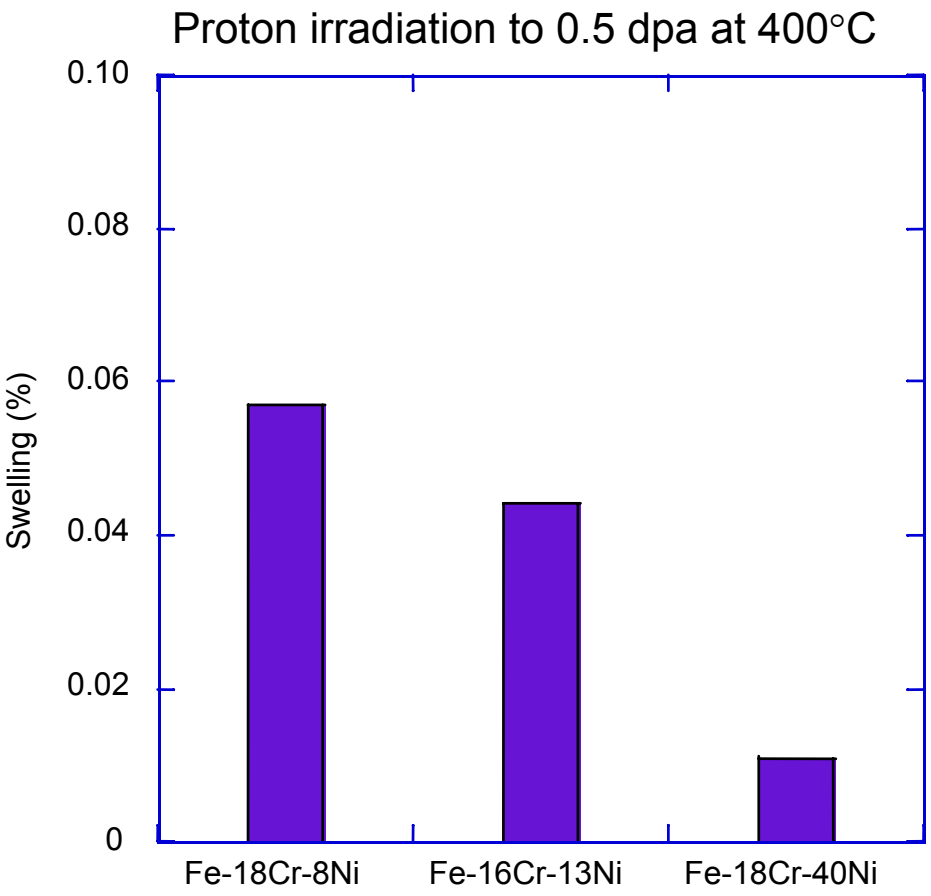

Figure 4.2 Swelling decrease with increasing bulk nickel concentration.

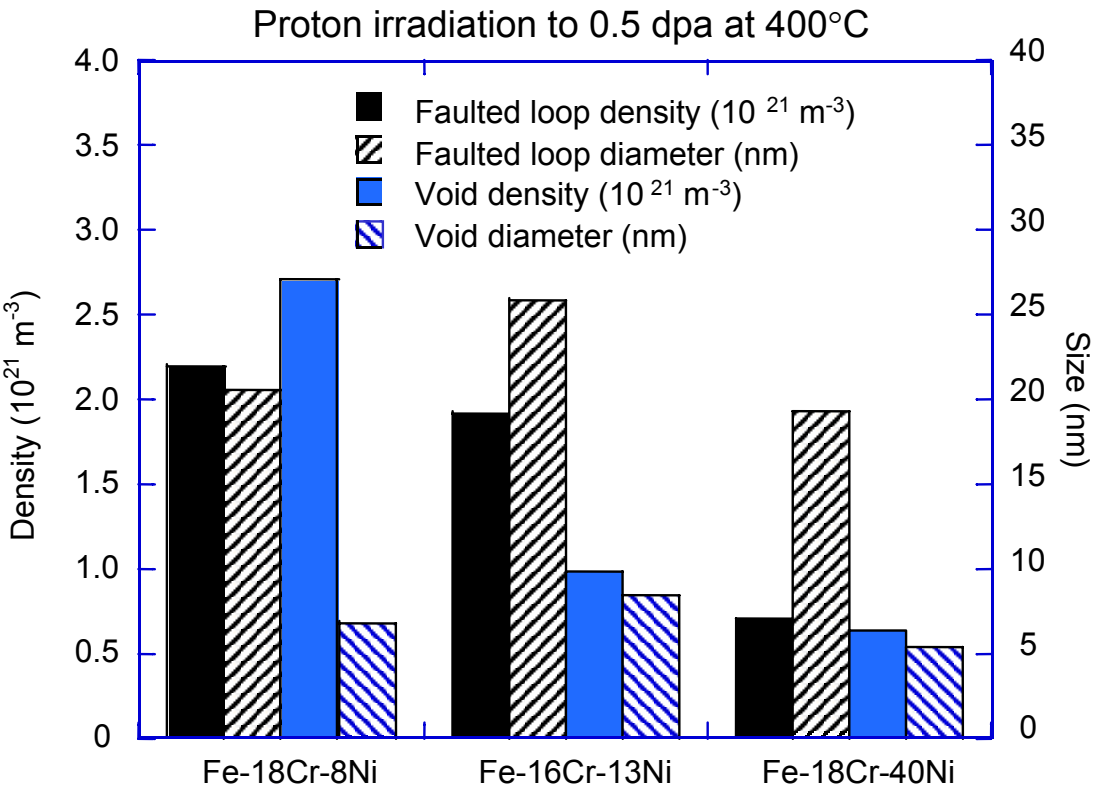

Figure 4.3 Microstructural changes with increasing bulk nickel concentration.

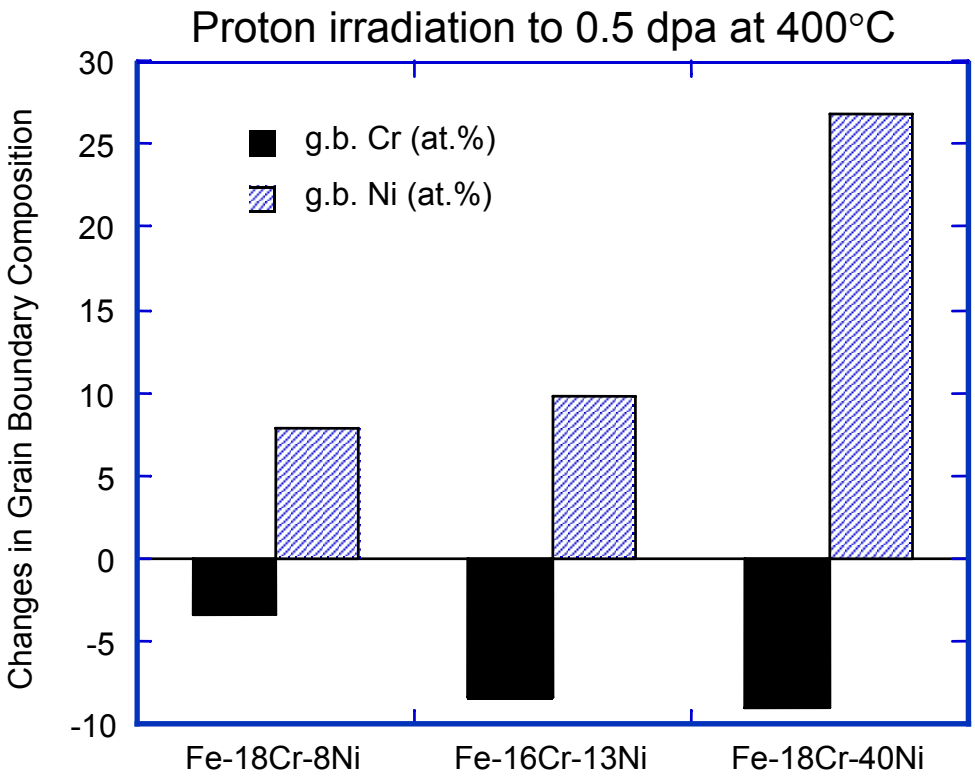

Figure 4.4 Changes in grain boundary composition with increasing bulk nickel concentration.

4.1.2 Effect of Adding Mo and P to a 316 Base Alloy

Figure 4.5 indicates the change in hardness with the addition of the minor elements molybdenum and phosphorus to the 316 base (Fe-16Cr-13Ni-1.25Mn) alloy irradiated to 0.5 dpa. The addition of molybdenum has little effect on hardening, while the addition of phosphorous causes a significant increase. Figure 4.6 indicates that the addition of molybdenum had little effect on swelling while the addition of phosphorus dramatically decreases swelling. For the phosphorous doped alloy, no voids were seen.

The microstructural changes in the 316-series are shown in figure 4.7. The addition of molybdenum does not have a strong effect on either the loop or void distributions. The most

dramatic effect is the complete lack of voids in the phosphorous doped alloy. To a dose of 0.5 dpa, no voids were visible.

The radiation-induced grain boundary segregation for the 316 series is shown in figure 4.8. As with the microstructural development, the addition of molybdenum does not have a dramatic effect, but the addition of molybdenum plus phosphorus did. The alloy with molybdenum plus phosphorus had much smaller chromium depletion and nickel enrichment than the other alloys in the series.

A comparison between the nickel series and the 316 series indicates an interesting relationship between the 40 wt, % nickel alloy and the molybdenum plus phosphorus alloy. Both were successful in reducing the amount of void swelling. The 40 wt. % nickel alloy had a large amount of radiation-induced chromium depletion and nickel enrichment while the molybdenum plus phosphorus alloy did not. The molybdenum plus phosphorus alloy actually reduced the RIS. Each was successful in reducing swelling, but likely through a different mechanism. No voids were found in the molybdenum plus phosphorus alloy, indicating that the phosphorus may tie up point defects and prevent a significant number of vacancies from grouping to nucleate voids. The 40 wt. % nickel alloy had voids, but at a lower density possibly indicating the large amount of segregation hindered voids from reaching the critical size for sustained growth. Note that in the literature, the effect of phosphorus on suppressing voids in neutron-irradiated stainless steels is typically explained by needle-shaped phosphorus precipitates, different from our work where no phosphorus precipitates were observed.

Stress corrosion cracking tests were performed in the 316 series. The results are shown in figure 4.9. The addition of molybdenum resulted in a significant increase in the amount of cracking. However the addition of molybdenum and phosphorus reduced the amount of cracking to a level comparable to the base alloy. The underlying cause of the variations in cracking with alloying addition is not clear. The amount of chromium depletion was smaller but the amount of hardening was greater in the molybdenum plus phosphorus alloy than in the molybdenum alloy. This indicates chromium depletion may be more critical for this system, but a conclusion would require a broader dataset.

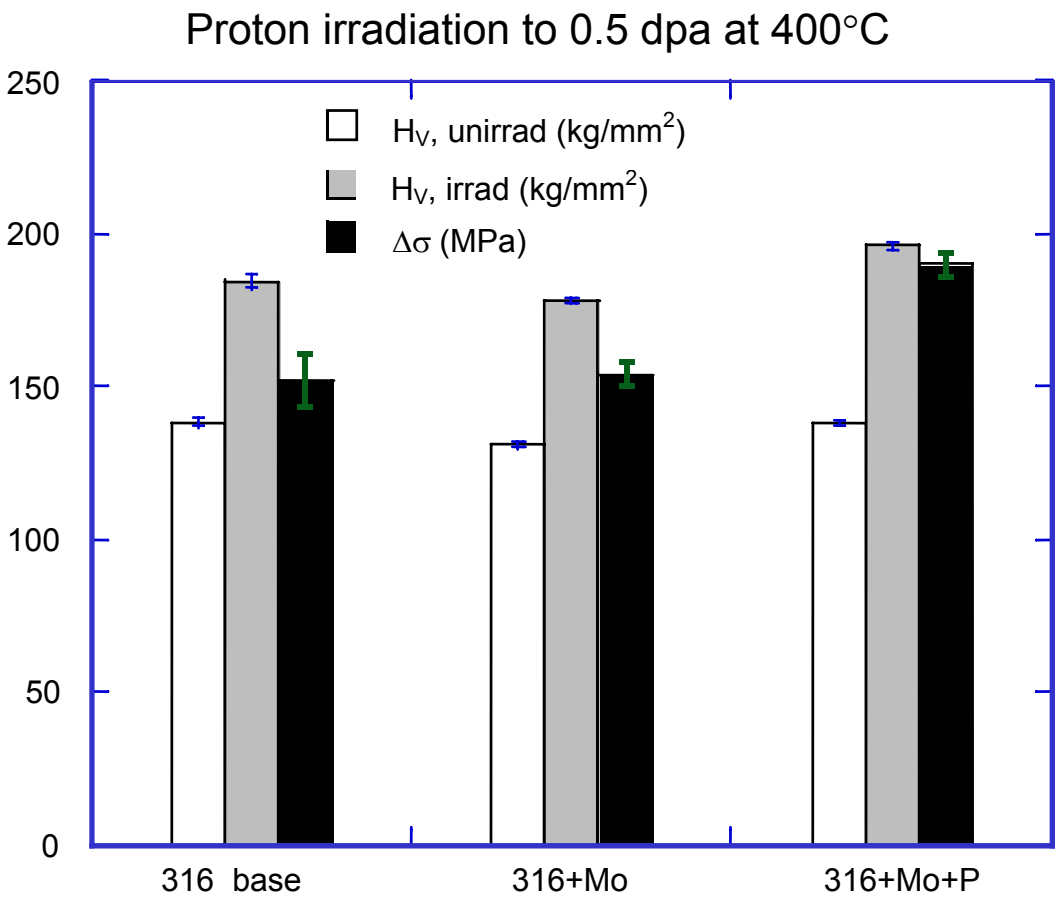

Figure 4.5 Hardness change in the Fe-16Cr-13Ni-1.25Mn alloy plus the addition of minor elements Mo and P.

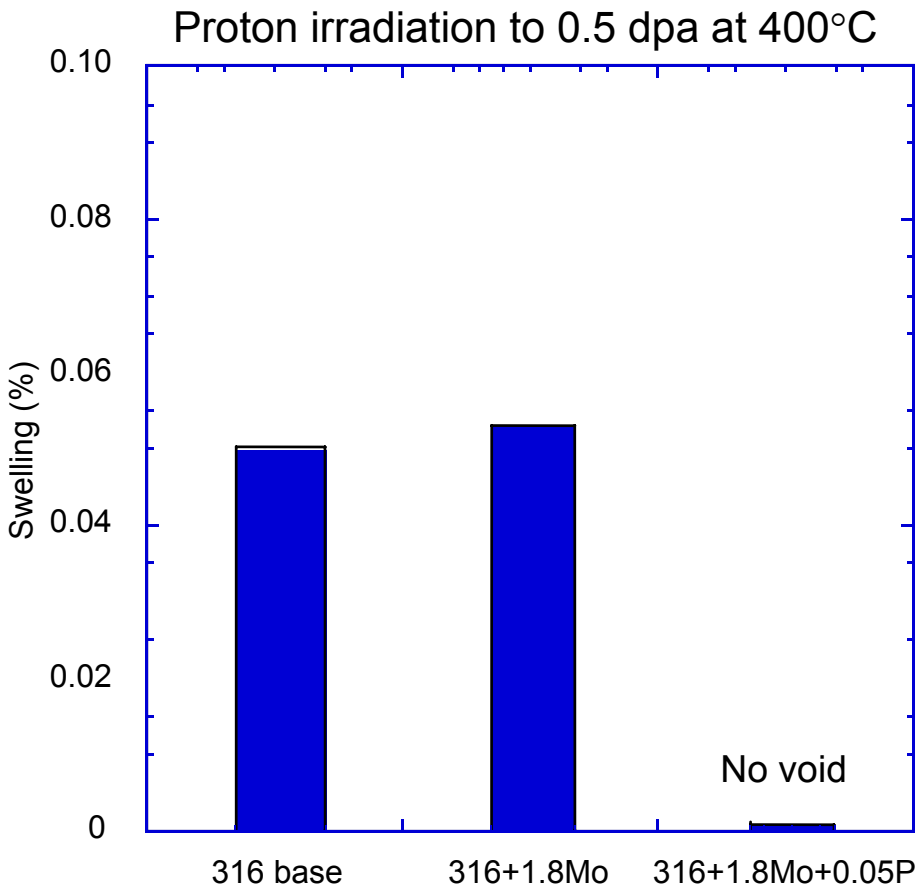

Figure 4.6 Swelling in the Fe-16Cr-13Ni-1.25Mn alloy plus the addition of minor elements Mo and P.

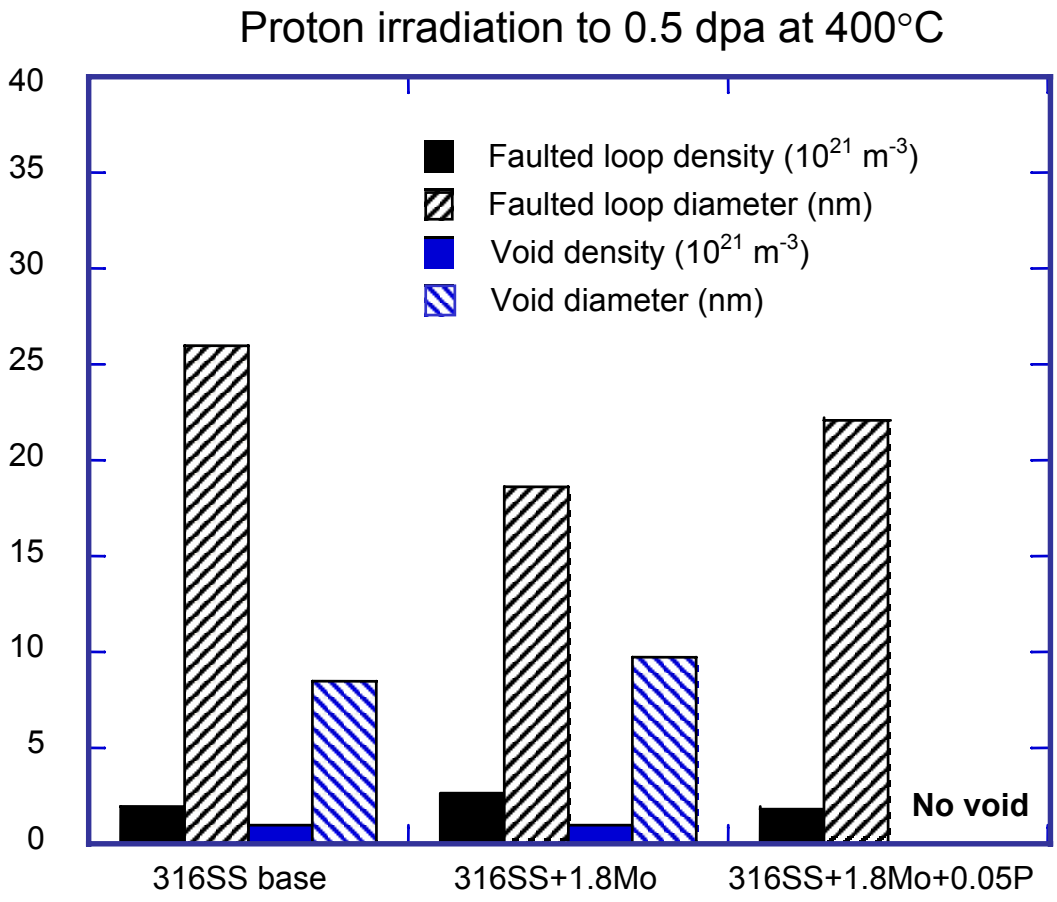

Figure 4.7 Microstructural changes in the Fe-16Cr-13Ni-1.25Mn alloy plus the addition of minor elements Mo and P.

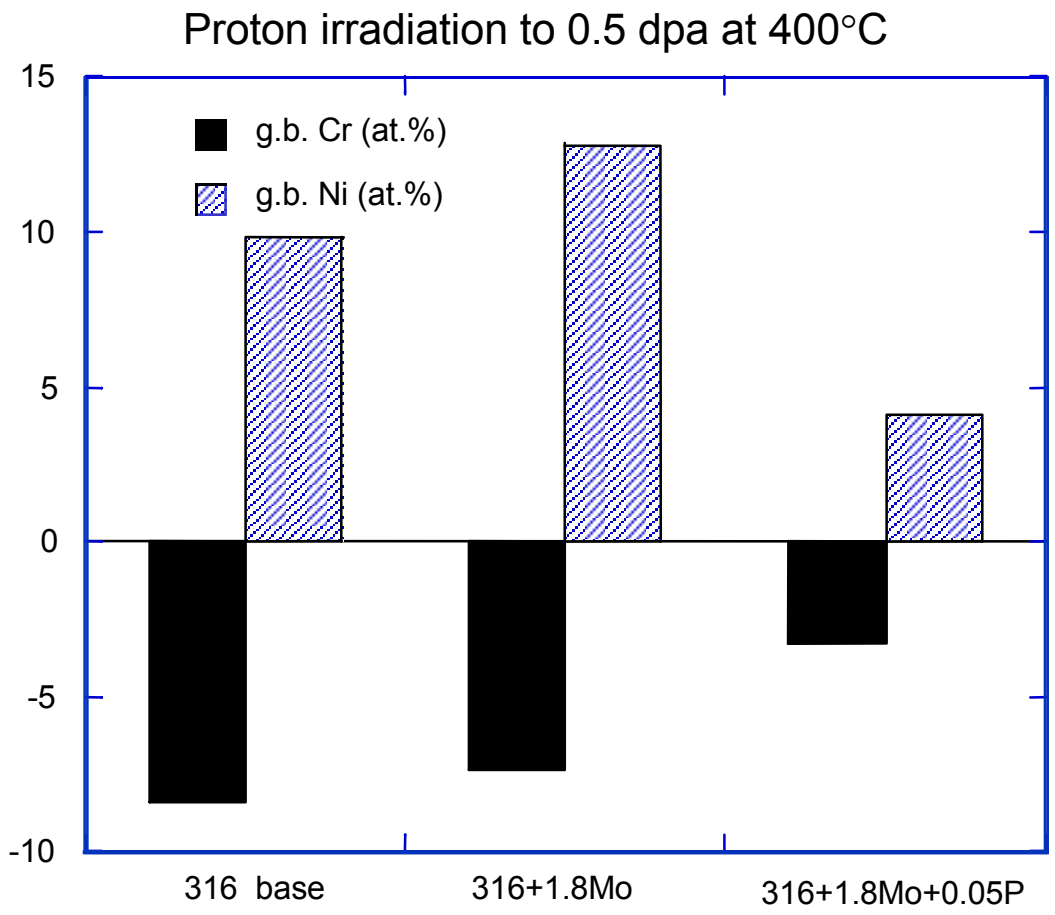

Figure 4.8 Grain boundary segregation in the Fe-16Cr-13Ni-1.25Mn alloy plus the addition of minor elements Mo and P.

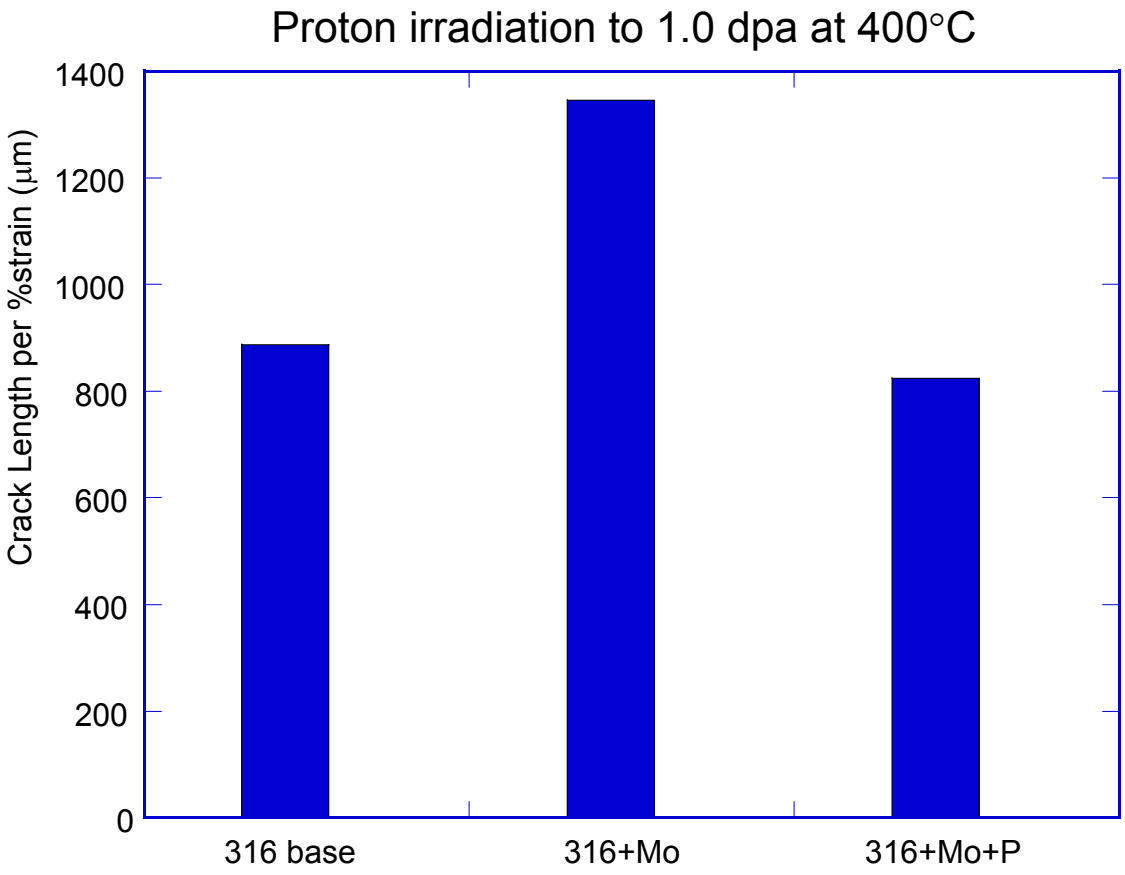

Figure 4.9 Stress corrosion cracking test results in the Fe-16Cr-13Ni-1.25Mn alloy plus the addition of minor elements Mo and P.

4.1.3 Effect of Adding the Oversized Element Zr

The effect of adding two different levels of zirconium to an Fe-18Cr-9Ni-1.75Mn alloy is shown in figure 4.10. Both zirconium-containing alloys hardened less than the base alloy. The swelling as a function zirconium concentration is shown in figure 4.11. The addition of zirconium decreases the swelling with a greater decrease occurring at higher zirconium levels. From both a swelling and irradiation hardening perspective, the addition of zirconium appears to be beneficial. Two important items should be noted. First, additional zirconium can be added before zirconium phases are expected to precipitate, so additional experimentation with higher zirconium levels will be pursued. Second, the alloys in this study were purposely chosen to have

low carbon. Real engineering steels typically have carbon. The addition of carbon, which might tie up zirconium in carbide phases, may make preparation of zirconium-doped alloys more difficult.

The microstructural development for alloys doped with zirconium is seen in figure 4.12. The density and average size of the frank loops and voids are shown. Similarly to the nickel series, the main effect of the addition of zirconium is to reduce the density of voids and loops. No consistent effect of zirconium concentration on size was noted. The grain boundary segregation as a function of zirconium concentration is displayed in figure 4.13. Increasing zirconium concentration from 0.04 wt. % to 0.16 wt. % increased the segregation slightly. The zirconium alloys have a similar effect as increasing bulk nickel concentration in the nickel series. Decreasing swelling is associated with larger amounts of segregation.

Stress corrosion cracking tests were performed on the zirconium series. The results are displayed in figure 4.14. The stress corrosion cracking was worst in the base alloy, somewhat better in the high zirconium alloy and best in the low zirconium alloy. The results do agree with grain boundary chromium concentration in that the low zirconium alloy had less grain boundary chromium depletion than did the high zirconium alloy. But they run contrary to the hardening behavior.

The overall response from the zirconium containing alloys was positive. They improved the swelling and IASCC response while reducing the radiation hardening. Further study of zirconium alloys is recommended.

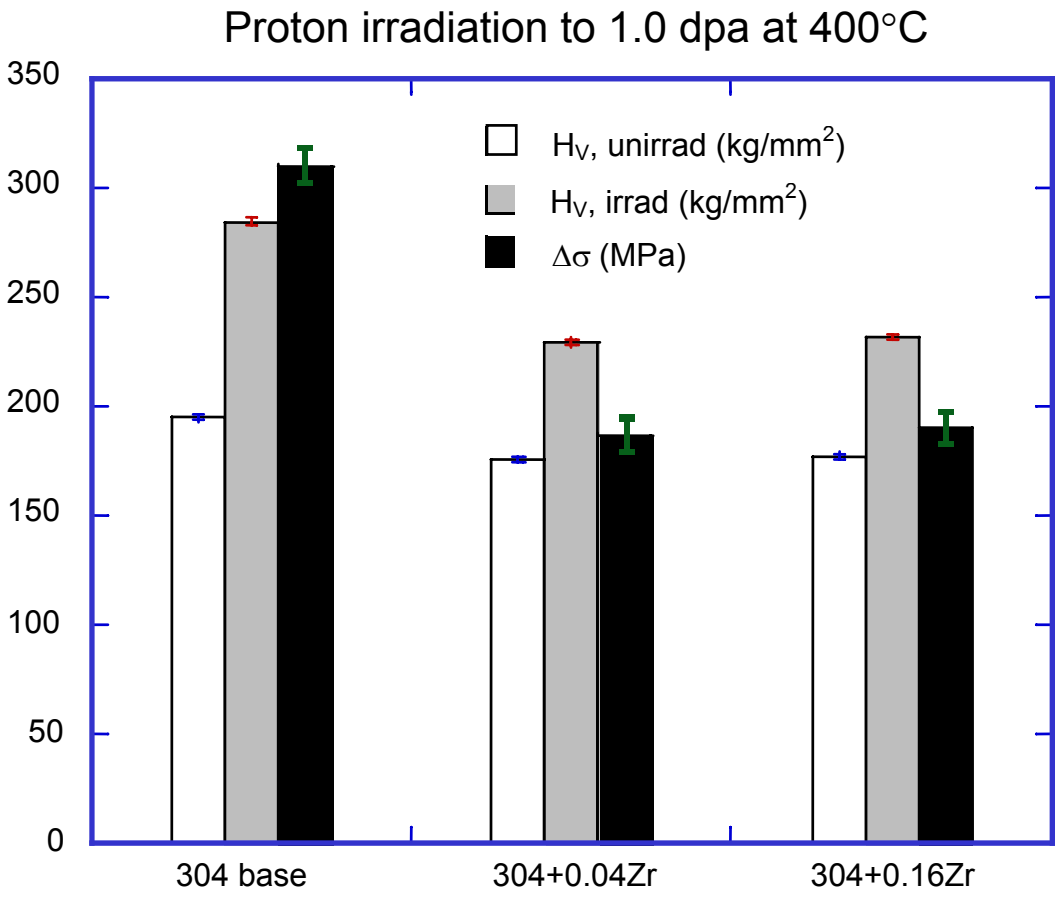

Figure 4.10 Effect of the addition of zirconium on hardening, the error bars indicating the standard deviation of the mean for the measurements.

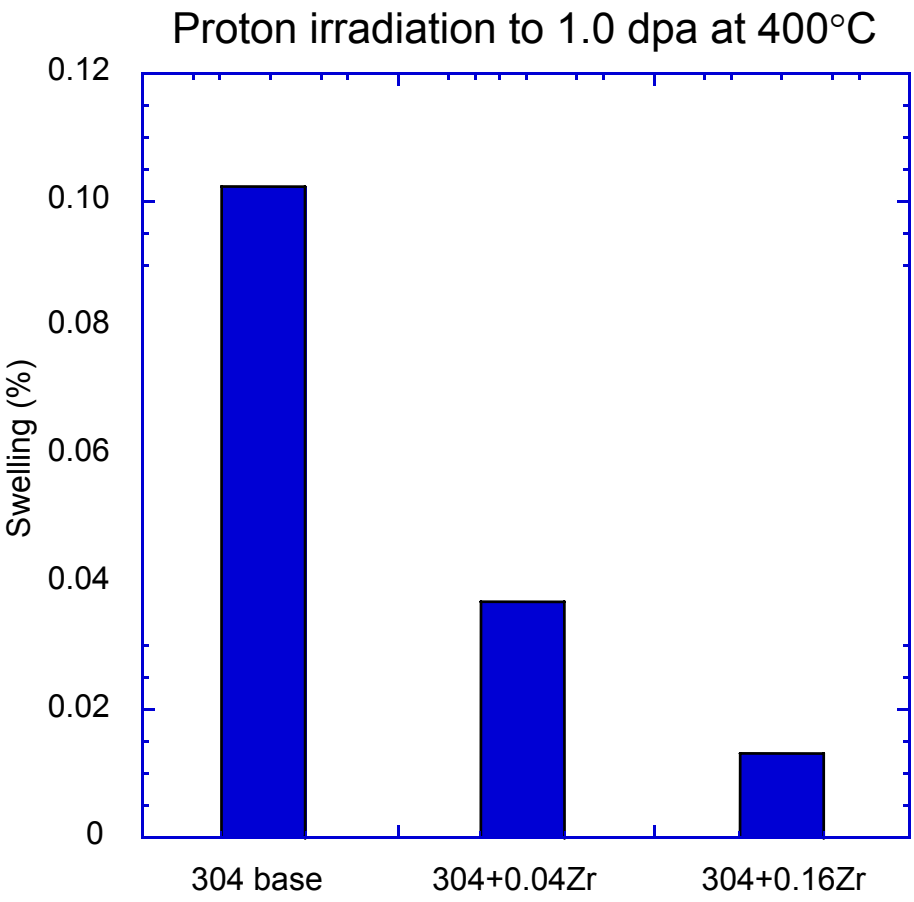

Figure 4.11 Effect of the addition of zirconium on swelling.

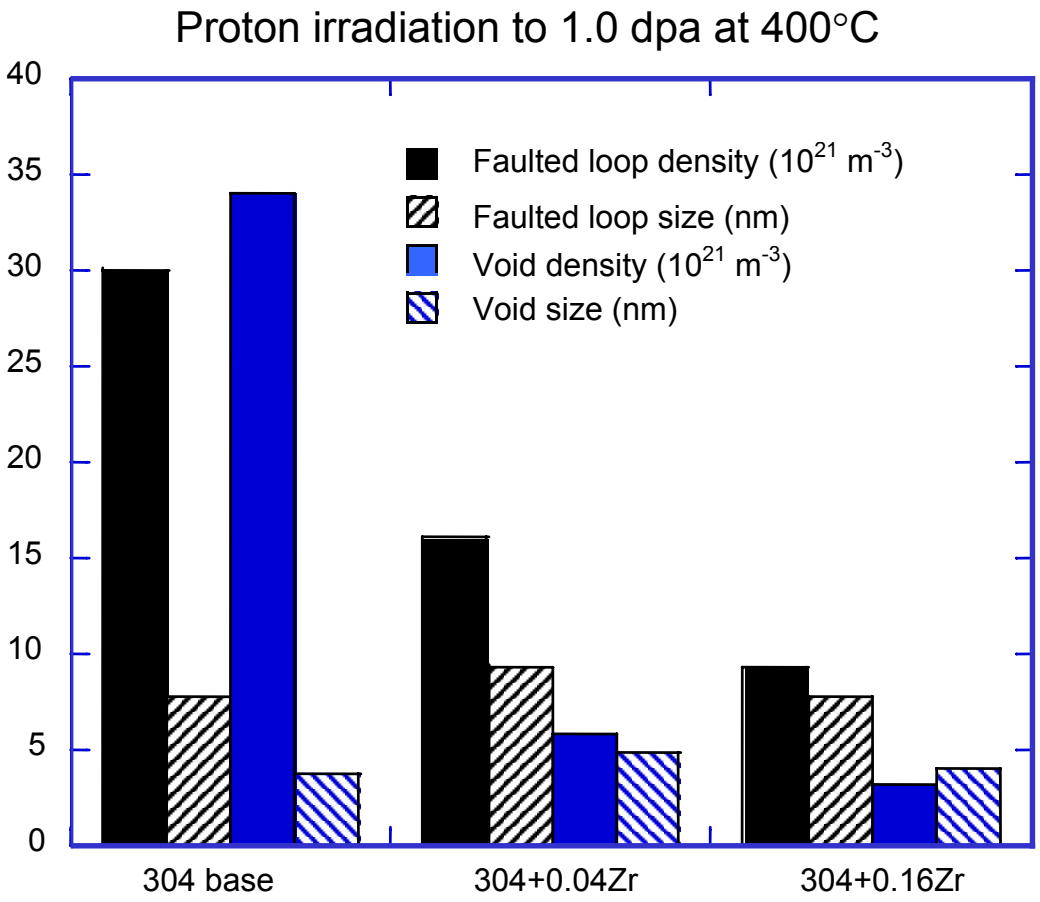

Figure 4.12 Effect of the addition of zirconium on microstructural development.

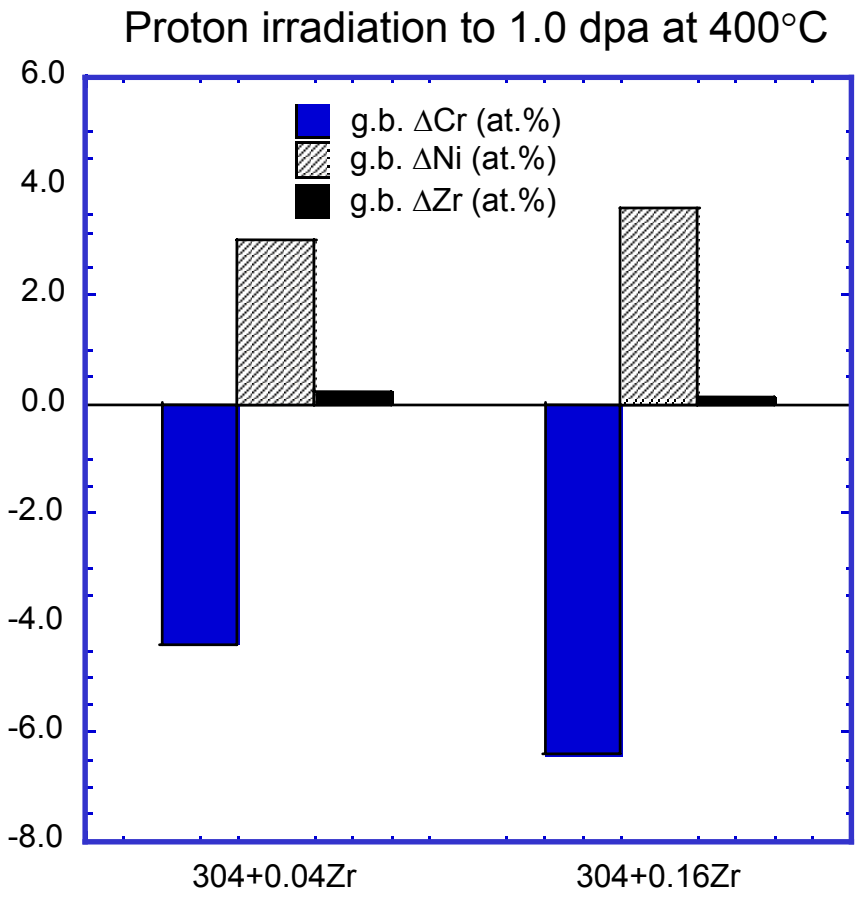

Figure 4.13 Effect of the addition of zirconium on radiation-induced grain boundary segregation.

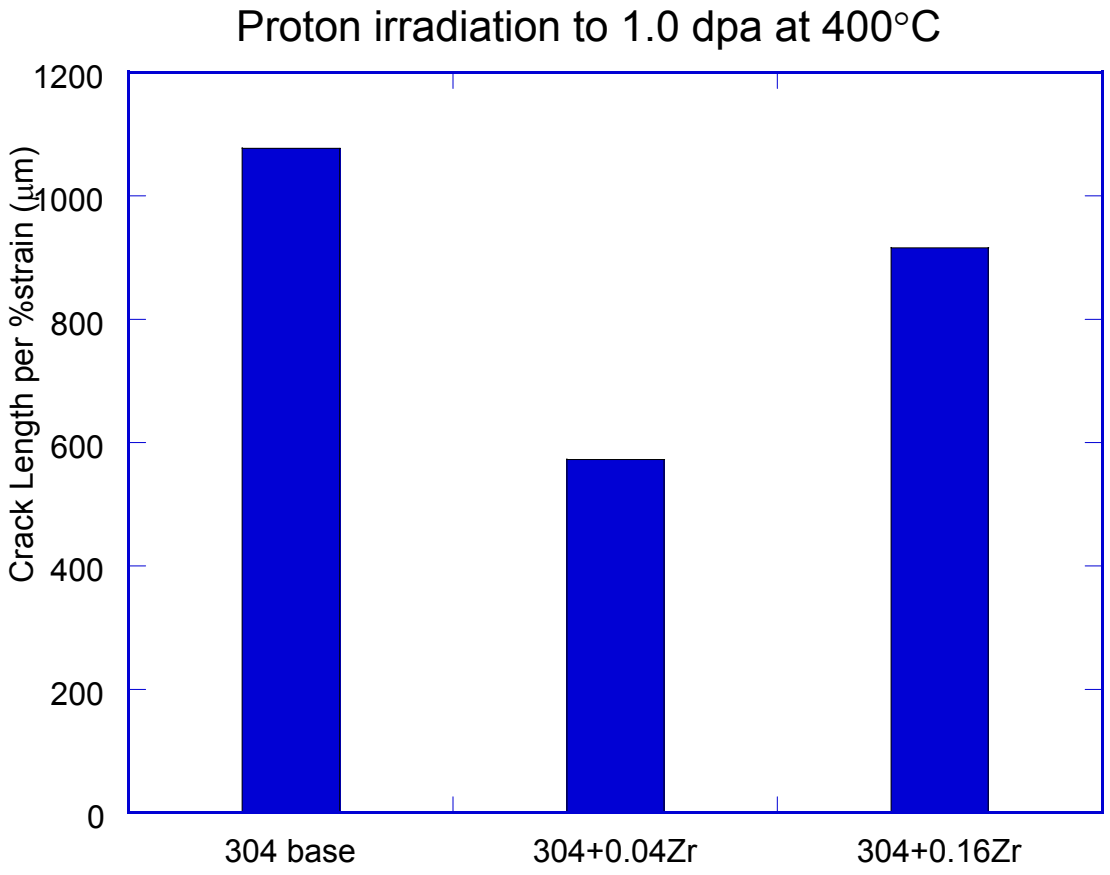

Figure 4.14 Effect of the addition of zirconium on IASCC.

4.2. Grain Boundary Compositional Engineering

Figure 4.15 provides the basis for the grain boundary composition engineering (GBCE) studies performed in this study. During irradiation, atoms couple with the vacancy and interstitial fluxes in such a manner that certain items are drawn toward the boundary (enrichment) and others away (depletion). This is known as radiation-induced segregation. For radiation-induced segregation in Fe-Cr-Ni alloys, chromium always depletes and nickel always enriches.

When a metal alloy is heated to high temperature and then cooled slowly, a flux of vacancies drifts toward the grain boundaries. Atoms can couple preferentially with the vacancy flux drawing atoms toward the boundary. Experimental evidence shows that chromium will enrich

under these conditions. The goal in the grain boundary compositional engineering studies is to determine a heat treatment and cooling sequence that maximizes the grain boundary chromium concentration at the grain boundary prior to irradiation, thus delaying the chromium depletion during irradiation.

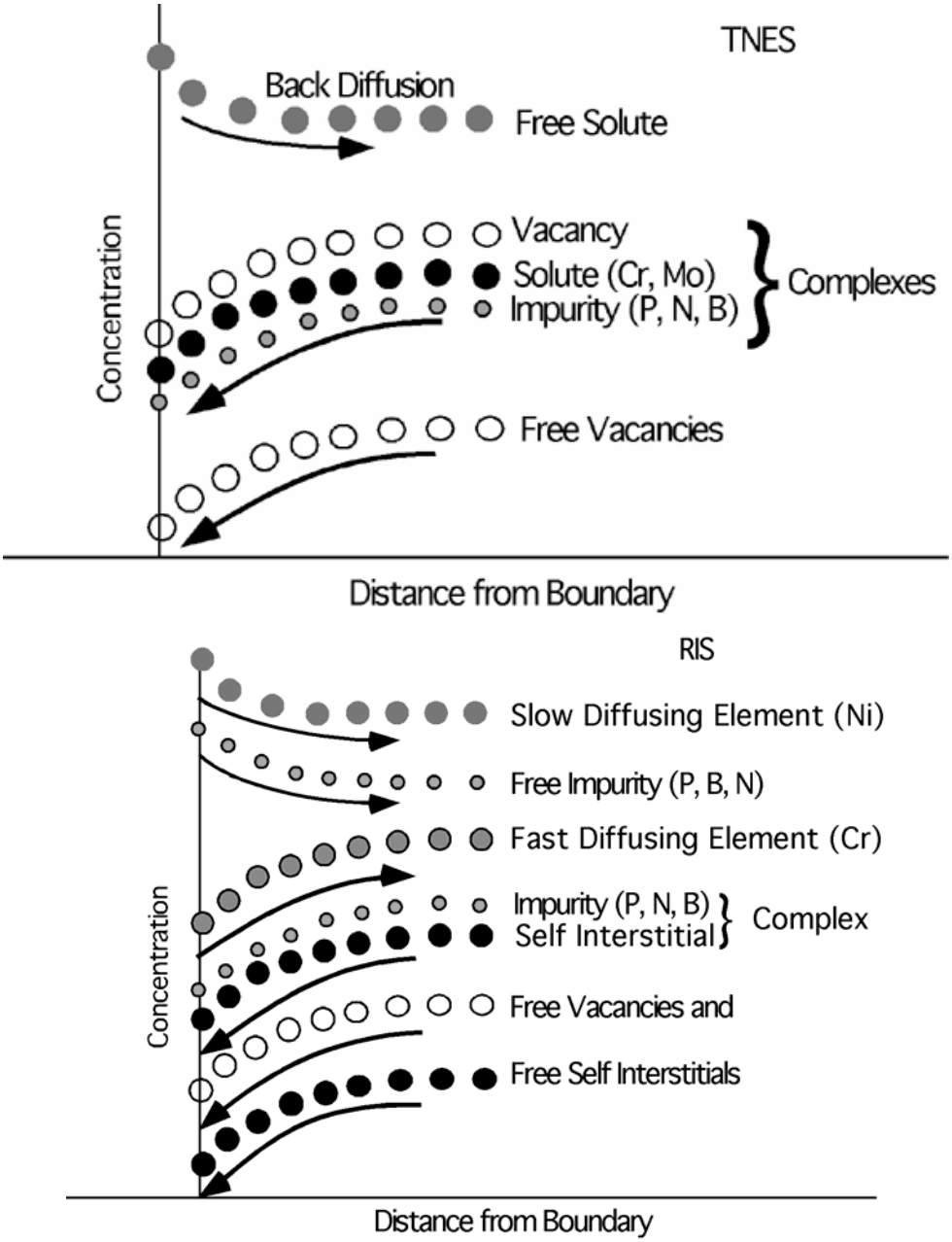

Figure 4.15 Schematic diagrams of Thermal non-equilibrium segregation (TNES) and radiaiton-induced segregation (RIS).

Thermal non-equilibrium segregation is different from RIS in two significant ways. TNES occurs at higher temperatures and involves only vacancies, while RIS involves both vacancies and self –interstitial atoms. In addition, vacancy concentrations for TNES are much lower than point defect concentrations generated during RIS. Formation of vacancy concentrations during higher temperature annealing and their subsequent migration to sinks during cooling is believed to be the primary process leading to TNES [17]. As the material cools a vacancy concentration gradient develops between the grain boundaries, which act as sinks, and the matrix which has a supersaturation of vacancies. During cooldown, both free vacancies and vacancy-solute complexes will diffuse to the grain boundaries thus enriching the boundaries with the complexed element. Concentration gradients that form as a result of enrichment at the grain boundaries results in back diffusion of free solute at elevated temperature. If the material is quenched too fast, the supersaturated vacancies are frozen in the matrix and do not have an opportunity to diffuse to the boundary and produce TNES. On the contrary, if the sample is cooled too slowly, back diffusion of the free solute will eliminate the enrichment. Only at intermediate cooling rates is the enrichment optimized.

For the first series of studies to optimize enrichment (quench rate studies), a single alloy, base 316 + Mo + P, was selected. The effect of quench rate, annealing temperature and alloying were investigated to maximize the Cr enrichment at the grain boundaries.

Quench Rate:

To examine the effect of quench rate, samples of the base 316 + Mo + P alloy were heat treated at 1200°C for 1 hour and quenched or slowly cooled in several media to achieve different cooling rates. The four media chosen were: ice brine, room temperature water, air cooling, and furnace cooling. After heat treatment, the grains in the alloys were rather large, and typically only one to three grain boundaries could be observed in the thin regions of the TEM foil. Grain boundary chemistry profiles were measured for samples exposed to each of the four cooling rates. For each of the alloys examined, compositional differences between the grain boundary and the bulk were calculated. Grain boundaries showing the maximum segregation in each alloy were compared and these are listed in Table 3. The maximum was used as opposed to the

average because of the limited number of grain boundaries available for analysis and the observation that some of the boundaries that were analyzed showed no segregation. The absence of segregation in some boundaries may be an indication that these boundaries were twin boundaries which typically do not exhibit segregation. The results indicate that Cr, Mo and P are enriched at the grain boundaries, while Fe and Ni are depleted. A graphical representation of the Cr and Mo enrichment as a function of quench rate in the 316 + Mo + P alloy is provided in Figure 4.16. Both the furnace cooled and air cooled samples had similar amounts of Cr enrichment, so both alloys were selected for the next phase of the study.

Table 4.1 Maximum change in grain boundary composition compared to bulk composition for model 316 + Mo + P alloy as a function of quench media.

Treatment Parameters	Fe	Cr	Ni	Mo	P
1200°C, 1 hr, Brine	-1.62	0.43	-0.13	1.29	0.03
1200°C, 1 hr, Water	-5.69	1.82	2.20	1.63	0.02
1200°C, 1 hr, Air	-4.73	2.50	0.07	2.10	0.05
1200°C, 1 hr, Furnace	-7.30	2.63	1.24	3.33	0.10

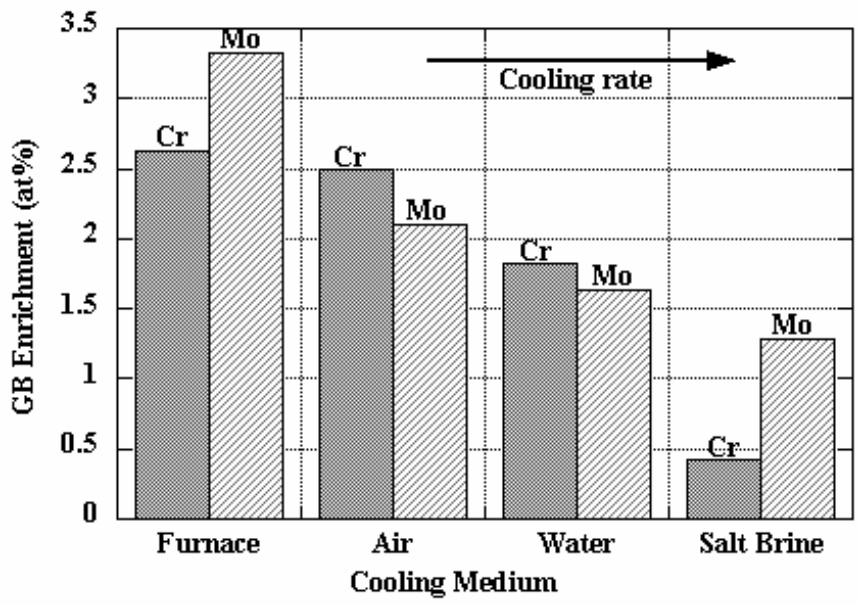

Figure 4.16 Effect of cooling rate on extent of grain boundary elemental enrichment in Fe-16Cr-13Ni + Mo + P annealed at 1200°C for 1 hour.

Annealing Temperature Studies:

To examine the effects of annealing temperature on grain boundary segregation, the base 316 + Mo + P alloy was annealed at 1100°C and 1300°C for 15 minutes prior to furnace and air cools. TEM samples were then examined as before using the FEG/STEM. The measured bulk versus grain boundary compositional differences are listed in Table 4.2. From the data, it is evident that the optimum treatment conditions are an 1100°C anneal for 15 minutes followed by air-cooling. On average these parameters produced the greatest amount of Cr segregation to the grain boundary. It should also be noted that the furnace cooled sample showed more grain boundary Mo segregation. A graphical representation of the Cr and Mo enrichment as a function of annealing temperature in the 316 + Mo + P alloy is provided in Figure 4.17.

Table 4.2 Change in grain boundary composition compared to bulk composition for model 316 + Mo + P alloy as a function of annealing temperature.

Treatment Parameters	Fe	Cr	Ni	Mo	P
1100°C, 15 min., Air	-6.28	4.79	-1.60	2.97	0.12
1100°C, 15 min., Furnace	-5.81	2.48	-1.14	4.35	0.13
1300°C, 15 min., Air	-3.55	1.47	0.31	1.71	0.06
1300°C, 15 min, Furnace	-7.58	2.53	1.39	3.57	0.09

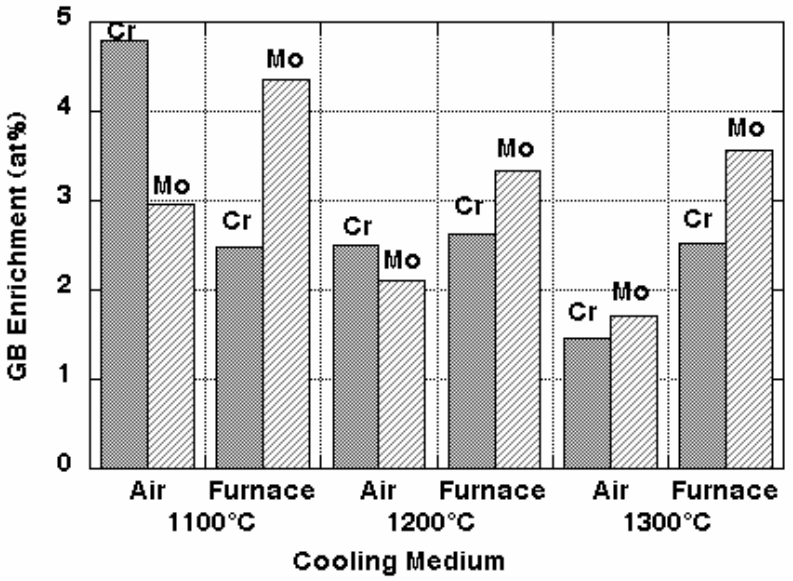

Figure 4.17 Grain boundary Cr and Mo enrichment as a function of annealing temperature.

Alloying Effects:

Following development of the optimum heat treatment (1100°C for 15 minutes followed by air-cooling) to Cr enrich the boundaries, the treatment was performed on the base 316, base 316 + Mo alloy and base 316 + Mo + P alloys. Typical segregation profile plots, measured using FEG-STEM, from the base 316, base 316 + Mo and base 316 + Mo + P with enriched grain boundaries are shown in Figure 4.18. The plots illustrate that Cr enrichment can occur in the simplest alloy (base 316) to a comparable extent as alloys containing alloying additions such as Mo and P. The extent of Fe depletion and Ni enrichment in the base 316 alloy was less than the other two alloys. As with the base 316 + Mo + P, substantial enrichment of Mo also occurs in the base 316 + Mo.

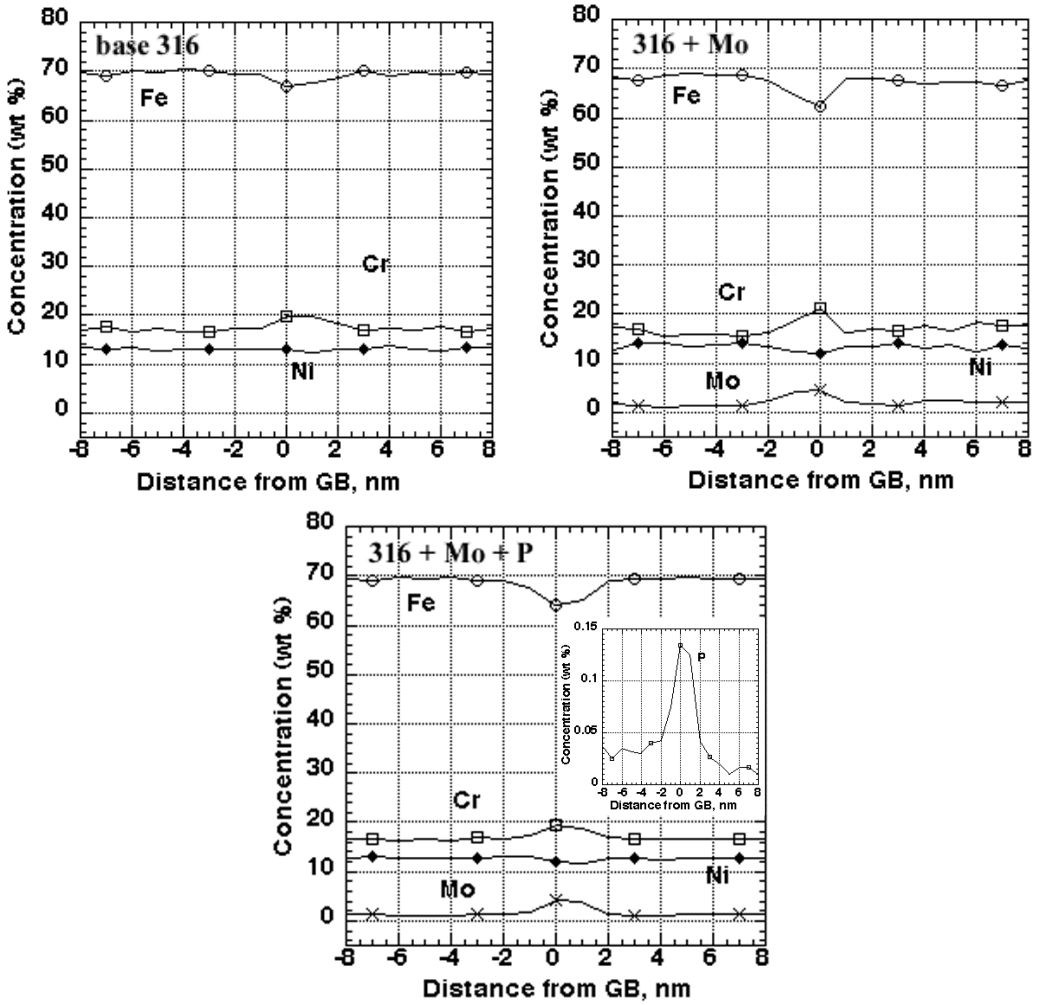

Figure 4.18 Segregation profiles for the 316 series of alloys following heat treatments to Cr enrich the grain boundaries. Inset in 316 + Mo + P plot shows P enrichment.

Radiation-Induced Segregation Behavior

As described earlier, molybdenum additions did not have a significant impact on the swelling and RIS behavior of the 316 series model alloys. The addition of phosphorus did lead to a substantial refinement of the dislocation microstructure, suppression of void formation, and a reduction in the extent of Cr depletion at grain boundaries. A plot of grain boundary Cr depletion and Ni enrichment as a function of composition in the model 316 SS alloys is shown in Figure 4.18. P enrichment in the proton irradiated samples was at a similar level to the sample heat treated to Cr enrich the grain boundary, indicating that grain boundary P levels do not significantly change as a result of RIS.

Figure 4.19 shows a comparison of segregation profiles in the proton irradiated base 316 + Mo with and without the heat treatment designed to Cr enrich the grain boundaries. It should be noted that even though the dose for the sample without Cr enriched boundaries was half the dose of the sample with the enriched boundaries, the extent of grain boundary Cr depletion was actually greater. In the enriched sample, a W shaped profile forms and Cr depletion at the grain boundary is reduced compared to the un-enriched boundary. In addition, the Fe and Ni show evident W profiles. However, the Mo profile is less conclusive, and it appears the rate at which the Mo is depleting is substantially greater than the Cr.

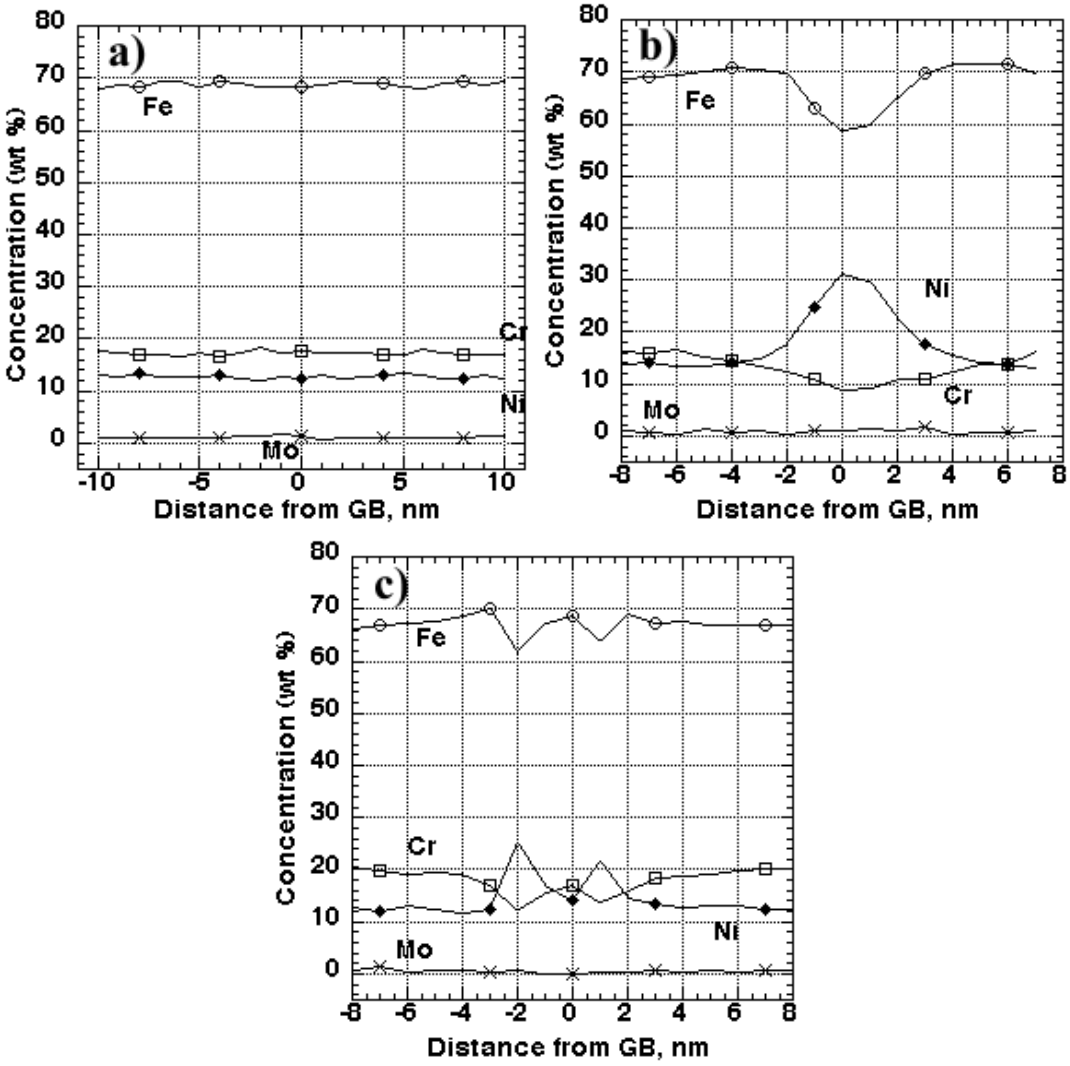

Figure 4.19 Segregation profiles for the 316 + Mo alloy a) without heat treatment, unirradiated, b) without heat treatment, proton irradiated to 0.5 dpa at 400°C c) with heat treatment, proton irradiated to 1 dpa at 400°C.

Stress corrosion cracking tests were performed on the base 316, 316+Mo and 316+Mo+P alloys heat treated to produce Cr pre-enrichment at grain boundaries. The results are displayed in Figure 4.20. The amount of cracking per unit strain is higher in GBCE alloys. Consistent with SCC behavior of the recrystalization heat treated alloys, the GBCE alloy with Mo+P performed better than that with only Mo added. These results indicate that GBCE treatment was not effective in reducing the amount of SCC in this environment. However, it should be noted that

the amount of grain boundary Cr depletion is very small in all cases, and other factors may play a larger role in influencing the SCC behavior.

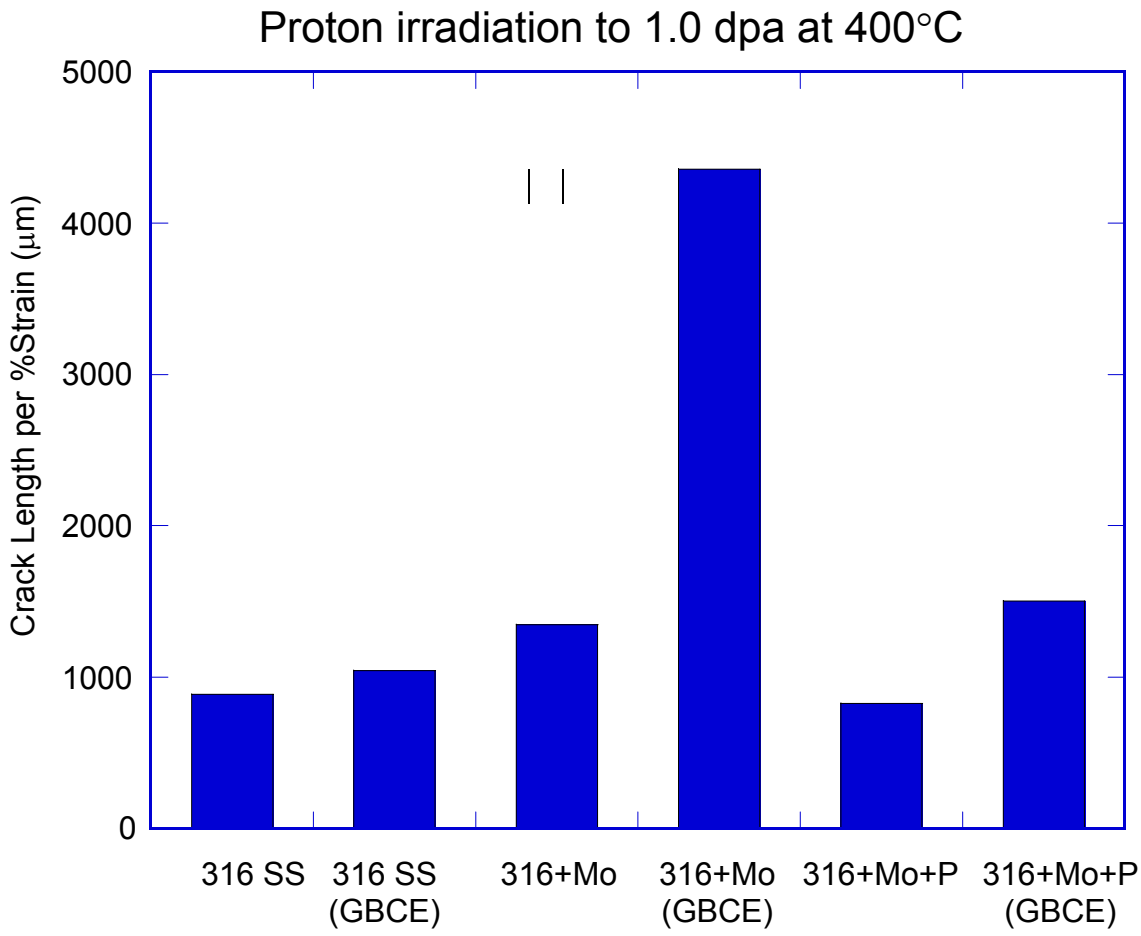

Figure 4.20 Effect of grain boundary composition engineering (GBCE) on IASCC of base 316, 316+Mo and 316+Mo+P irradiated with protons to 1 dpa at 400°C.

4.3. Grain Boundary Structural Engineering

Thermal mechanical treatments were developed to enhance the fraction of CSL boundaries. After recrystalization, the material underwent a compressive deformation followed by a heat treatment. Various tests conducted for CSL enhancement were listed in Table 4.3 for base 304 and 304+0.16Zr alloys and in Table 4.4 for base 316 and 316+Mo+P alloys. The boundaries with a Σ value greater than 1 and less than 37 were counted as CSL boundaries. The optimum

condition in comparison to the recrystalization treated condition is listed in Table 4.4. The fraction of high angle boundaries (HAB) decreased after a thermal mechanical treatment in addition to a recrystalization heat treatment. A reduction in HAB, which had been proven effective in resistance to thermal creep, may also improve the compositional stability under irradiation, therefore improving the resistance to RIS and possible intergranular cracking.

Table 4.3 Various thermal mechanical tests to enhance the fraction of CSL and HAB boundaries of the base 304 and 304+0.16Zr alloys.

Sample	Alloy	Heat Treatment	CSL(%)	HAB(%)
1810-T-8-1	Fe-18Cr-8Ni-1.75Mn	Ref	36.9	63.1
1812-C-Ref-0	Fe-18Cr-8Ni-1.75Mn+0.16Zr	Ref	28.3	71.7
1810-T-8-1-CSLE	Fe-18Cr-8Ni-1.75Mn	Ref+10%CW+975°C, 1 hr	47.7	52.3
1810-S-8-1-CSLE	Fe-18Cr-8Ni-1.75Mn	Ref+10%CW+975°C, 1 hr	51.1	48.9
1812-S-9-1-CSLE	Fe-18Cr-8Ni-1.75Mn+0.16Zr	Ref+10%CW+975°C, 1 hr	53.2	46.8

Table 4.4 The effect of CSL enhancement treatment on the fraction of CSL and HAB boundaries of the base 316 and 316+Mo+P alloys.

Sample	Alloy	Heat Treatment	CSL(%)	HAB(%)
1638-C-Ref-0	Fe-16Cr-13Ni-1.25Mn	Ref	41.1	58.9
1640-C-Ref-0	Fe-16Cr-13Ni-1.25Mn+P,Mo	Ref	55.8	44.2
1638-S-7-1-CSLE	Fe-16Cr-13Ni-1.25Mn	Ref+13%CW+925C, 15 min	58.3	41.6
1638-S-9-1-CSLE	Fe-16Cr-13Ni-1.25Mn	Ref+13%CW+925C, 15 min	76.7	23.3
1640-S-9-1-CSLE	Fe-16Cr-13Ni-1.25Mn+P,Mo	Ref+13%CW+925C, 15 min	44.8	55.2

The effect of CSL enhancement on the material response to radiation damage is demonstrated in Figure 4.21 where the result of post-irradiation SCC tests (1.0 dpa) in 288ºC normal water chemistry for base 304 and base 316 with and without CSL enhancement are compared. The sample treated with CSL enhancement prior to irradiation failed at a strain approximately two times of that without CSL enhancement. The beneficial effect of CSL enhancement is clearly demonstrated for base 304 irradiated to a dose of 1.0 dpa. Comparing SCC results in Figures 4.20 and 4.21 suggests that CSL enhancement has a stronger effect on improving SCC performance than does grain boundary Cr pre-enrichment. The effect of CSL enhancement on RIS is still under investigation and it is expected that CSL boundaries will develop less RIS, therefore improving material resistance to radiation damage.

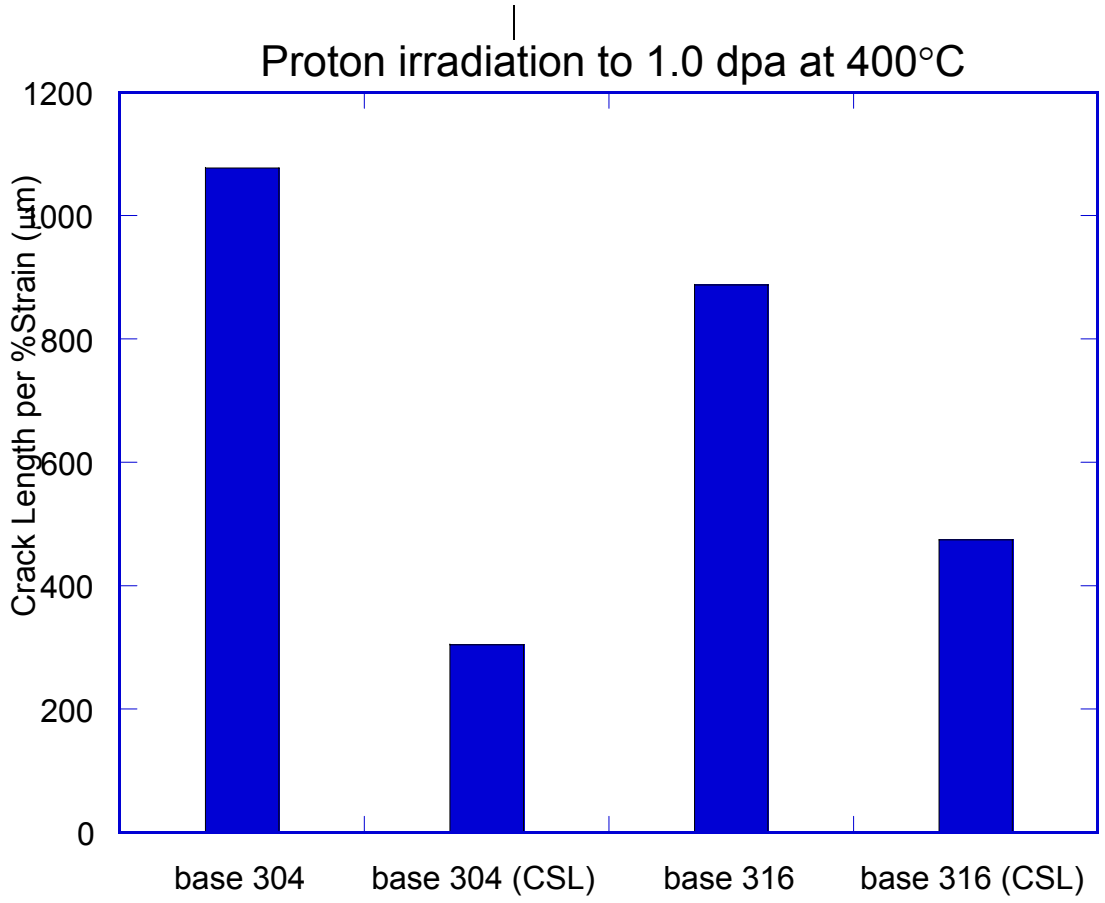

Figure 4.21 The effect of CSL enhancement on post-irradiation SCC test for base 304 and 316 alloys irradiated with protons at 400°C to a dose of 1.0 dpa.

4.4 Relationship between Composition, Swelling, and Radiation-induced Segregation

Void swelling occurs due to the nucleation and then growth of voids. At lower dose, the difference in void swelling is expected to be driven by the void nucleation and evidenced by differences in void density. At higher doses, the void distribution will essentially have nucleated and the difference in swelling between alloys is expected to be driven by the growth of voids.

In the Ni-series, 316 -series, and Zr-series, the systematic difference in the void swelling was due to differences in the void density and not the void size. Since these alloys were only radiated to 0.5 or 1 dpa, relatively low doses, the difference being driven by void density is not surprising. A simple analysis describes how changing composition can effect void nucleation and void density. For a system where point defect recombination is the dominant mechanism for the loss of point defects (in materials with a low point defect sink density), the steady-state concentration of vacancies C_v is given by [19]:

$$C_v = \sqrt{\frac{GD_iZ_i}{RD_vZ_v}}, \qquad (1)$$

where

Z_I and Z_v are the capture efficiencies for interstitials and vacancies, G is the radiation-induced vacancy creation rate, D_I and D_v are the diffusion coefficients for vacancies and interstitials, R is the vacancy-interstitial recombination constant where $R=4\pi r(D_I+D_v)$ and r is the radius of the recombination volume. Equation (1) describes the vacancies that are free to diffuse and nucleate voids. As can be seen, the following changes can decrease the concentration of vacancies and thus decrease the void nucleation rate:

1. Decrease the point defect creation rate
2. Decrease the interstitial diffusion coefficient (D_I is always greater than D_v so this is not a strong effect as the term $D_I + D_v$ appear in R)
3. Decrease the interstitial capture efficiency
4. Increase the vacancy diffusion coefficient
5. Increase the vacancy-interstitial recombination volume
6. Increase the vacancy capture efficiency

This study provided information on the effect of increasing vacancy diffusion rate. In the Ni-series, increasing the bulk nickel concentration increases the vacancy diffusion coefficient D_v.

This reduces the available vacancies, thus reducing the vacancy nucleation rate. As expected, the alloys with greater bulk nickel concentration have the lower void density.

The change in composition around the void due to radiation-induced segregation is expected to affect the void nucleation and growth. Segregation to the void surface has two potential effects [20]. If the segregation tends to increase the vacancy diffusion rate, then voids will grow more rapidly. Alternately, if the segregated region around a void is stiffer (has a larger elastic constant), then the void nucleation and growth rate will increase because a stronger repulsion of interstitials increases the bias for vacancies toward the void. This change in elasticity effects the bias for interstitials relative to vacancies.

For the Ni-series, RIS causes enrichment of nickel and depletion of chromium and iron. Moving toward higher nickel concentration increases the vacancy diffusion rate near the void. The increased vacancy diffusion rate causes the segregation profiles to reach steady-state faster. Measurements of segregation in Fe-18Cr-8Ni and Fe-20Cr-24Ni do show that increasing the bulk nickel content does decrease the time to steady-state segregation [21]. If segregation was the only effect, the segregation would increase the void growth rate. On the contrary, the effect of increasing bulk nickel concentration to decrease swelling has been shown at doses up to 140 dpa [1]. This indicates that the increased vacancy diffusion rate at void surfaces due to segregation is not likely to be a primary effect.

Wolfer et al. showed that a compositional change which increases the shear modulus or lattice parameter locally around a void embryo causes the void to become a preferential sink for vacancies, thus increasing the void nucleation rate [22-24]. For Fe-Cr-Ni alloys with compositions near 304/316 stainless steel, the lattice parameter and shear moduli increase with increasing Cr concentration and decrease with increasing Ni concentration [22]. For 304/316 stainless steel, RIS causes Cr to deplete and Ni to enrich around a void during irradiation. These changes in lattice parameter and shear modulus would tend to mitigate void nucleation. The smaller void density for alloys with greater bulk nickel concentration support the contention that increased shear modulus caused by RIS mitigates void nucleation. The data from the Ni-series

supports that concept that the likely dominant effect of RIS on void growth is through the effect on the elastic constants.

For the Zr-series, the effect of adding an oversized solute is thought to be to trap point defects. In this case, equation 1 is no longer strictly valid as it was derived assuming no traps. The effect of adding traps though is to decrease the concentration of point defects free to diffuse and thus nucleate a void. The addition of zirconium does decrease the void density, supporting the idea that Zr acts as a vacancy trap. Like the Ni-series, the reduction of vacancies free to diffuse does not eliminate radiation-induced segregation at grain boundaries. The reduction in point defect concentration may increase the rate at which the segregation reaches steady-state. Calculations indicate that for decreasing dose rate (and thus decreased free point defects), the segregation reaches steady-state more rapidly (Figure 4.22).

The parallel between the Ni-series and the Zr-series is interesting. For the Ni-series, increasing bulk nickel decreased swelling while increasing chromium depletion and nickel enrichment. Increasing vacancy diffusion rates leads to a lower concentration of freely migrating vacancies, causing the void nucleation rate to decrease, and decreasing the time to reach steady-state segregation. For the Zr-series, increasing bulk zirconium decreased swelling while increasing chromium depletion and nickel enrichment. Trapping of point defects leads to a lower concentration of freely migrating vacancies, causing the void nucleation rate to decrease, and decreasing the time to reach steady-state segregation.

The addition of Mo+P to the base 316 alloy decreases swelling but also decreases segregation. This is different than the Ni-series and the Zr-series. No voids were seen in the Mo+P alloy, indicating an effective method for prevention of void nucleation. Watanabe et al. [25], based on data from electron irradiations of Fe-Cr-Ni-P alloys, postulated a strong vacancy-phosphorus interaction that reduced the void swelling compared to alloys without the phosphorous. Similarly to the Zr-series, the vacancy trapping could reduce the vacancies free to diffuse and thus reduces the void nucleation rate.

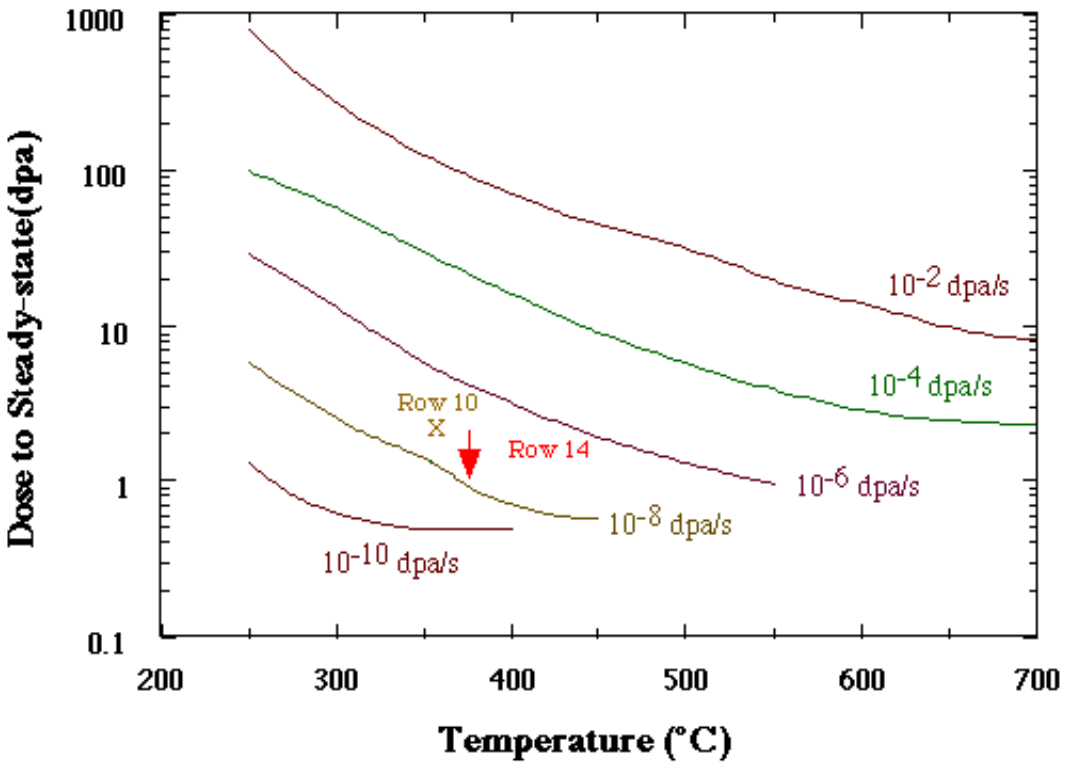

Figure 4.22 Effect of damage rate on time to reach steady-state radiation-induced segregation. Steady-state segregation occurs faster at lower rate.

A difference between the 316 series and the Zr-series is the chromium depletion and nickel enrichment. In the Zr-series, significant segregation of both chromium and nickel occurred while the segregation in the 316+Mo+P alloy was much smaller. As discussed earlier, trapping vacancies lowers the concentration of vacancies free to diffuse and cause segregation, also decreasing the time to steady-state RIS. This effect alone would not decrease segregation as seen in the 316+Mo+P alloy. Therefore, the addition of P must alter the relative diffusion rates of iron, chromium, and nickel to reduce the segregation. Both chromium and phosphorous and molybdenum and phosphorous are known to have attractive potentials [26]. The addition of phosphorus, which enriches at the boundary, may act as a pin for chromium and molybdenum, thus reducing the depletion.

Previous work by Damcott et al. [27], showed that the addition of P to an Fe-18Cr-8Ni alloy increased both the chromium enrichment and nickel depletion. Therefore, adding P alone

appears to increase segregation while the addition of Mo and P decrease the segregation. The attractive force is greater between Mo and P than between Cr and P. Apparently, the addition of Mo is critical to decreasing the overall segregation.

The entire discussion above on the relationship between voids and segregation must be taken in context. The analysis is based on samples irradiated at a single temperature and dose. To get a full understanding of the effects requires a broader range of irradiation conditions.

4.5 Relationship between Irradiated Microstructure and IASCC

The effect of combining grain boundary engineering and bulk composition engineering on the IASCC behavior of the 304 SS alloy is shown in Table 4.5. The Zr doped alloys demonstrated reduced crack length per unit strain as well as decreased total crack length, and increased strain to failure. The use of CSL enhancement also resulted in a significant increase in the strain to failure and a reduction in the number of cracks and the total crack length per unit strain. The combination of bulk addition of Zr and grain boundary engineering resulted in the least crack length per unit strain. The 304+Zr+CSLE sample demonstrated superior performance over the 304+CSLE sample with respect to total crack length and crack length per unit strain. The 304+Zr+CSLE sample performed better than the 304+Zr sample with respect to total crack length, crack length per unit strain, and maximum strain tolerance. The increase in hardness of the 304+Zr+CSLE was comparable to the 304+Zr alloy. The behavior of the 304+Zr+CSLE sample indicates that Zr doping and CSL enhancement may be combined to achieve increased IASCC resistance. While the addition of Zr and CSL enhancement separately improve the cracking resistance, the combination of the two provides the greatest effect.

Table 4.5 Combined effect of Zr addition, CSL enhancement in 304SS and Mo+P addition, GBCE and CLSE in 316SS.

Alloy condition	Max. strain (%)	Total crack length (μm)	Crack length/unit strain (μm)
304 base	11.44	12323	1077
304+CSLE	16.33	4960	304
304+0.16Zr	9.82	9000	916
304+0.16Zr+CSLE	15.00	1940	129
316+Mo+P	8.49	6992	824
316+Mo+P+GBCE	10.7	16054	1500
316+Mo+P+GBCE+CSLE	In autoclave	In autoclave	In autoclave

4.6 Examining traditional theories of IASCC

Traditional thinking on IASCC holds that both grain boundary chromium depletion and matrix hardening can contribute to IASCC. In this work, many different alloys and processing conditions were irradiated and tested. Examining IASCC susceptibility (as measured using crack length per unit strain) as a function of grain boundary chromium depletion and matrix hardening provide data to examine these traditional theories.

Figure 4.23 plots crack length per unit strain versus chromium depletion for those samples where RIS measurements exist. No apparent trend exists between cracking susceptibility and RIS. The most susceptible alloy was the 316+Mo alloy heat treated to pre-enrich chromium.

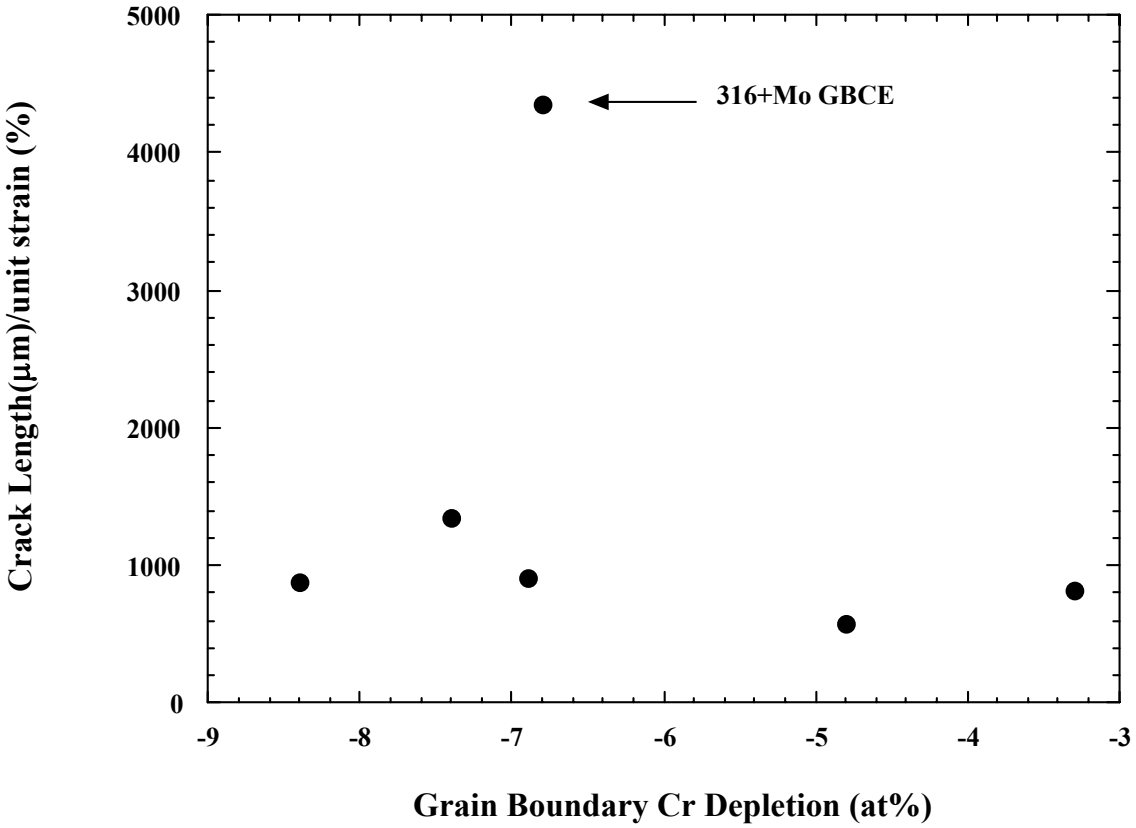

Figure 4.23 IASCC susceptibility versus grain boundary chromium depletion.

Figure 4.24 plots crack length per unit strain versus change in hardness. Three key points are noted. First, there is no general trend of greater susceptibility with greater hardness. For the alloys examined, there is no apparent relationship between cracking and hardness. Second, the worst susceptibility occurs in the 316+Mo sample that has been heat treated to pre-enrich chromium at the grain boundary. The most resistant alloy is the base 304 alloy that has been treated to minimize the fraction of high angle boundaries. This 304+CSL alloy, with the greatest resistance, has the greatest hardness. The resistance of the CSL enhanced sample indicates that grain boundary properties may be more important than bulk properties. Unfortunately, RIS measurements were not taken on the 304 CSL sample after irradiation.

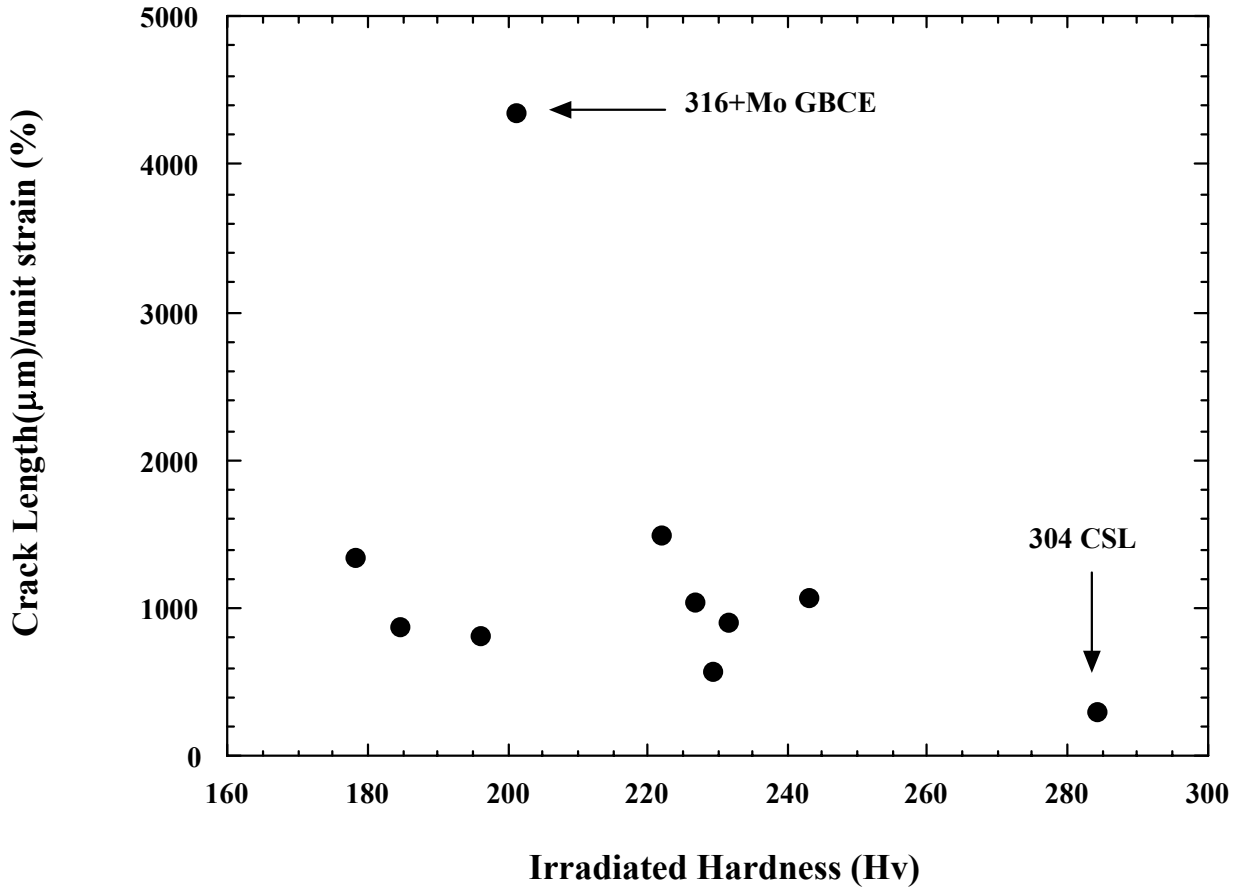

Figure 4.24 IASCC susceptibility versus hardness.

4.7 Irradiation Plan

Based on the results of this experimental program, the following materials were identified for reactor testing. The materials were chosen either because a specific treatment looked promising (addition of Zr of grain boundary structure engineering) or to further examine a surprising result (brain boundary composition engineering).

Fe-18Cr-9.5Ni-1.75Mn
Fe-18Cr-9.5Ni-1.75Mn+0.04Zr
Fe-18Cr-9.5Ni-1.75Mn+0.16Zr

Fe-16Cr-13Ni-1.25Mn (g.b. Cr pre-enrichment treatment)
Fe-16Cr-13Ni-1.25Mn+Mo (g.b. Cr pre-enrichment treatment)
Fe-16Cr-13Ni-1.25Mn+Mo+P (g.b. Cr pre-enrichment treatment)

Fe-18Cr-9.5Ni-1.75Mn (g.b. CSL enhanced)
Fe-16Cr-13Ni-1.25Mn (g.b. CSL enhanced)

5.0 Conclusions

Three major directions were researched to improve the radiation resistance of nuclear energy system structural materials: bulk composition engineering, grain boundary composition engineering, and grain boundary structure engineering. For bulk composition engineering, three groups of alloys were investigated. One looked at the effect of increasing bulk nickel to alloys with 16-18 Cr, one at the effect of the alloying additions Mo and P to a base 316 alloy, and one the effect of the addition of the oversized element Zr to a base 304 alloy. For grain boundary composition engineering, the effect of enriching chromium at grain boundaries prior to irradiation was examined. For grain boundary structure engineering, the effect of minimizing the fraction of high angle boundaries was studied.

In each case, material modifications were made and the radiation response of the material both with and without the modifications was characterized. Radiation was performed using 3.2 MeV protons at 400°C. The post irradiation characterization was performed using multiple measures including: hardness, microstructural characterization, grain boundary composition measurements, and stress corrosion cracking resistance testing.

The effect of increasing bulk nickel concentration for alloys with 16-18% bulk chromium was to decrease swelling, increase grain boundary segregation, and increase hardening. Although higher nickel is effective at decreasing swelling, the increased radiation hardening at greater bulk nickel concentrations is problematic. No further testing of this approach is anticipated.

The addition of Mo to a base 316 alloy had little effect on swelling, grain boundary segregation or hardening, but did increase the cracking. The addition of Mo and P had a significant effect, reducing swelling and segregation but increased the hardening. The addition of Mo and P had little effect on cracking. The study of the 316 series did provide some illumination on the reasons 316 performs better in an irradiation environment, but this alloy series is not expected to make major strides in radiation performance and no further study is anticipated.

The addition of zirconium to a base 304 alloy decreased swelling and hardening, but significant grain boundary segregation still occurred. The addition of Zr also improved the cracking resistance. Because of the positive results in every measure of radiation resistance, the addition of Zr to austenitic steels deserves further study.

In the grain boundary composition engineering studies, heat treatment conditions were optimized to enrich chromium at grain boundaries prior to irradiation. This pre-enrichment does delay the chromium depletion to higher dose, but these heat treatments did not lead to reduced cracking.

For the grain boundary structural engineering task, thermal mechanical treatments were performed to minimize the fraction of high angle grain boundaries. Decreasing the fraction of high angle boundaries did reduce the cracking susceptibility.

In a final test, the effect of Zr addition and the reduction of high angle grain boundaries were combined. Using both of these techniques was a greater improvement in cracking resistance than either technique alone. Further studies on oversized alloying additions and grain boundary structural engineering are both warranted.

6.0 Acknowledgments

Thanks to Peter Andresen and the General Electric Corporate Research and Development Laboratory who provided the alloys. Research at the Oak Ridge National Laboratory SHaRE User Facility was sponsored by the Division of Materials Sciences and Engineering, U. S. Department of Energy under contract DE-AC05-00OR22725 with UT-Battelle, LLC., and through the SHaRE Program under contract DE-AC05-76OR00033 with Oak Ridge Associated Universities.

7.0 References

[1] F. A. Garner, Irradiation Performance of Cladding and Structural Steels in Liquid Metal Reactors, in Materials Science and Technology, A Comprehensive Treatment, Vol 10A Nuclear Materials, Eds., R. W. Cahn, P. Haasen, and E. J. Kramer, (VCH Weinheim, 1994).

[2] S. M. Bruemmer, Private communication

[3] W. G. Johnston, J. H. Rosolowski, A. M. Turkalo, and T. Lauritzen, J. Nucl. Mater. 54 (1974) 24.

[4] D. L. Porter, G.L. McVay, and L. C. Walters, Effects of Radiation on Materials: Tenth Conference, ASTM-STP 725, David Kramer, H. R. Brager, and J. S. Perrin, Eds., American Society for Testing and Materials, pp.500-511.

[5] Y. Tanaka, S. Suzuki, M. Kodama, S. Nishimura, K. Fukuya, H. Sakamoto, K. Nakata, and T. Kato, Proceedings of the Eighth International Symposium on Environmental Degradation of Materials in Nuclear Power Systems-Water Reactors, American Nuclear Society, 1997, pp.803-811.

[6] T. Kato, H. Takahshi, and M. Izumiya, J. Nucl. Mater. 189 (1992). 167-174.

[7] G. S. Was, in Critical Issue Reviews for the Understanding and Evaluation of Irradiation-Assisted Stress Corrosion Cracking, Electric Power Research Institute, Palo Alto, EPRI TR-107159, 1996, p. 6-1.

[8] S. M. Bruemmer and E. D. Simonen, *Corrosion* 50 (1994) 940.

[9] G. S. Was, Cooperative IASCC Research (CIR) Program Meeting, Prague, Czech Republic, November, 1997.

[10] J. M. Cookson, R. D. Carter, D. L. Damcott, M. Atzmon and G. S. Was, J. Nucl. Mater. 202 (1993) 104.

[11] M. Kodama, K. Fukuya and H. Kayano, in Proc. 16th International Symposium on Effects of Radiation on Materials, Kumar, Gelles, Nanstead and Little, eds., ASTM, Philadelphia, 1994, p. 889.

[12] D. L. Damcott, J. M. Cookson, et al. Nucl. Inst. Meth. Phys. Res. B99 (1995). 780-783.

[13] H. R. Higgy, F. H. Hammad, J. Nucl. Mater., 55 (1975) 177.

[14] Christine Brown, Developments in Electron Microscopy and Analysis, Ed. J. V. Venables, Academic Press, 1976

[15] William and Carter, Transmission Electron Microscopy, Vol. III, Plenum Press, New York, 1996

[16] T. R. Allen, J. T. Busby, G. S. Was, and E. A. Kenik, *Effects of Radiation on Materials, 19th International Symposium, ASTM STP 1366,* M. L. Hamilton, A. S. Kumar, S. T. Rosinski, and M. L. Grossbeck, Eds., American Society for Testing and Materials, 1999.

[17] R. G. Faulkner, Int. Mat. Rev., **41 (5)** (1996) p. 198.

[18] J. I. Cole, T. R. Allen, G. S. Was, Y. Yang and E. A. Kenik, Proceedings of the Tenth International Conference on Environmental Degradation of Materials in Nuclear Power Systems-Water Reactors, NACE International, CD-ROM, Paper 31.

[19] L. K. Mansur, J. Nucl. Mater. (1994) 97.

[20] L. K. Mansur, Nucl. Tech. 40 (1978) 5.

[21] Allen, T. R., Busby, J. T., Gan, J., Kenik, E. A , and Was, G. S., "**The Correlation Between Swelling and Radiation-Induced Segregation in Iron-Chromium-Nickel Alloys**," *Effects of Radiation on Materials, 19th International Symposium, ASTM STP 1366,* M. L. Hamilton, A. S. Kumar, S. T. Rosinski and M. L. Grossbeck, Eds., American Society for Testing and Materials, West Conshohocken, PA, 1999.

[22] W. G. Wolfer, F. A. Garner, et al. *Effects of Radiation on Materials: Eleventh Conference, ASTM STP 782*, (American Society for Testing and Materials, 1982) p.1023.

[23] W. G. Wolfer and L. K. Mansur, J. Nucl. Mater. **91** 265 (1980).

[24] A. Si-Ahmed and W. G. Wolfer *Effects of Radiation on Materials: Eleventh Conference, ASTM STP 782, American Society for Testing and Materials* (1982), p.1008.

[25] H. Watanabe, A. Aoki, H. Murakami, T. Muroga, and N. Yoshida, J. Nucl. Mater. 155-57 (1988) 815.

[26] R. Guillou, M. Guttmann, and Ph. Dumoulin, Metal Science, (February 1981) 63.

[27] D. L. Damcott, J. M. cookson, R. d. Carter jr., J. R. Martin, M. Atzmon, and G. S. Was, Rad. Eff. And Def. in Solids, 118 (1991) 383.

8.0 Milestone Plan

Milestone/Task Description	Planned Completion Date	Actual Completion Date
Prepare sample alloys	Year 1	Year 1
Develop grain size thermo-mechanical treatments	Year 1	Year 1
Irradiate Ni-series alloys	Year 1	Year 1
Analyze Ni-series alloys	Year 1	Year 1
Irradiate 316-series alloys	Year 2	Year 2
Analyze 316-series alloys	Year 2	Year 2
Irradiate Zr-series alloys	Year 3	Year 3
Analyze Zr-series alloys	Year 3	Year 3*
Grain boundary Cr enrichment treatments	Year 2	Year 2
Irradiate and analyze grain boundary Cr enrichment treatments	Year 2	Year 3
CSLE enhancements	Year 2	Year 2
Irradiate and analyze enhanced samples	Year 3	Year 3*

* Including Extension